Journal of Inflammation Research

Dovepress
open access to scientific and medical research

Open Access Full Text Article

ORIGINAL RESEARCH

# Jintiange Capsule Alleviates Rheumatoid Arthritis and Reverses Changes of Serum Metabolic Profile in Collagen-Induced Arthritic Rats



Xiaoyan Wang,[1]* Yi Shen,[1]* Xinying Zhuang,[1] Na Wang,[2] Qi Zhang,[1] Lulin Zhu,[1] Yuling Liu,[1] Xinyu Lu,[1] Luping Qin,[1] Qiaoyan Zhang[1]

[1]School of Pharmaceutical Sciences, Zhejiang Chinese Medical University, Hangzhou, 310053, People's Republic of China; [2]Ginwa Enterprise (Group) INC, Xi'an, 710069, People's Republic of China

*These authors contributed equally to this work

Video abstract

Point your SmartPhone at the code above. If you have a QR code reader, the video abstract will appear. Or use: https://youtu.be/fgIlc5Wmw_Y

Correspondence: Qiaoyan Zhang; Luping Qin
Tel +86 571-6176 8519
Email zqy1965@163.com; lpqin@zcmu.edu.cn

**Purpose:** Jintiange capsule (JTG), an approved drug developed as a substitute for tiger bone (TB), has been clinically applied for osteoporosis therapy since 2003. The drug is composed of bionic TB powder, in which peptides and proteins are primarily enriched from other bone extracts. However, as a precious material of traditional Chinese medicine (TCM), TB has been mainly understood and used in TCM to relieve osteoporosis, rheumatoid arthritis and bone injury. Inspired by those, the purpose of this study was to investigate whether JTG also had an effect on relieving rheumatoid arthritis in collagen-induced arthritic (CIA) rats and explore potential mechanism from the perspective of serum metabolic profile changes.

**Methods:** JTG was analyzed using Nano LC-MS/MS and orally administered in CIA rats for 6 weeks. After administration, intervention effects of JTG on synovial inflammation, bone micro-architecture and bone metabolism were studied, and the impact of JTG on serum metabolic profiles in CIA rats was investigated by metabolomics.

**Results:** Nine bioactive peptides were identified in JTG. In animal treatments, JTG alleviated paw swelling ($P < 0.01$), arthritic severity ($P < 0.01$) and synovial tissue proliferation, as well as inflammatory cell infiltration of ankle joint, decreased bone loss, improved microstructure of bone in CIA rats by regulating bone absorption and formation, specifically increasing bone mineral density (BMD) ($P < 0.05$), bone volume fraction (BVF) ($P < 0.05$), trabecular number (Tb.N) ($P < 0.05$) and decreasing trabecular separation (Tb.Sp) ($P < 0.05$). Besides, serum IL-6 was down-regulated remarkably in CIA rats ($P < 0.05$). Furthermore, metabolomics analysis revealed that 32 metabolites were regulated significantly ($P < 0.05$) by comparison between CIA model and JTG in 360 mg/kg dose. The pathway analysis implied that JTG was involved in regulation of biosynthesis of phenylalanine.

**Conclusion:** JTG alleviates rheumatoid arthritis and reverses changes in serum metabolic profile in CIA rats.

**Keywords:** bionic tiger bone powder, synovial inflammation, bone micro-architecture, bone metabolism, metabolomics

## Introduction

Rheumatoid arthritis (RA) is a highly prevalent chronic, systemic and degenerative autoimmune disease accompanied by persistent synovitis (inflammation of the synovial membrane), emergence of cartilage erosion, and destruction of the bone and joints.[1] RA is pathologically heterogeneous, with many suspected triggers for the development of the disease, including environmental,[2] epigenetic,[3] and genetic factors[4–6] as well as several types of post-translational modifications of proteins.[7] Patients with RA typically have destruction of joint cartilage and bone accompanied

Received: 7 September 2021
Accepted: 22 November 2021
Published: 8 December 2021

**Graphical Abstract**

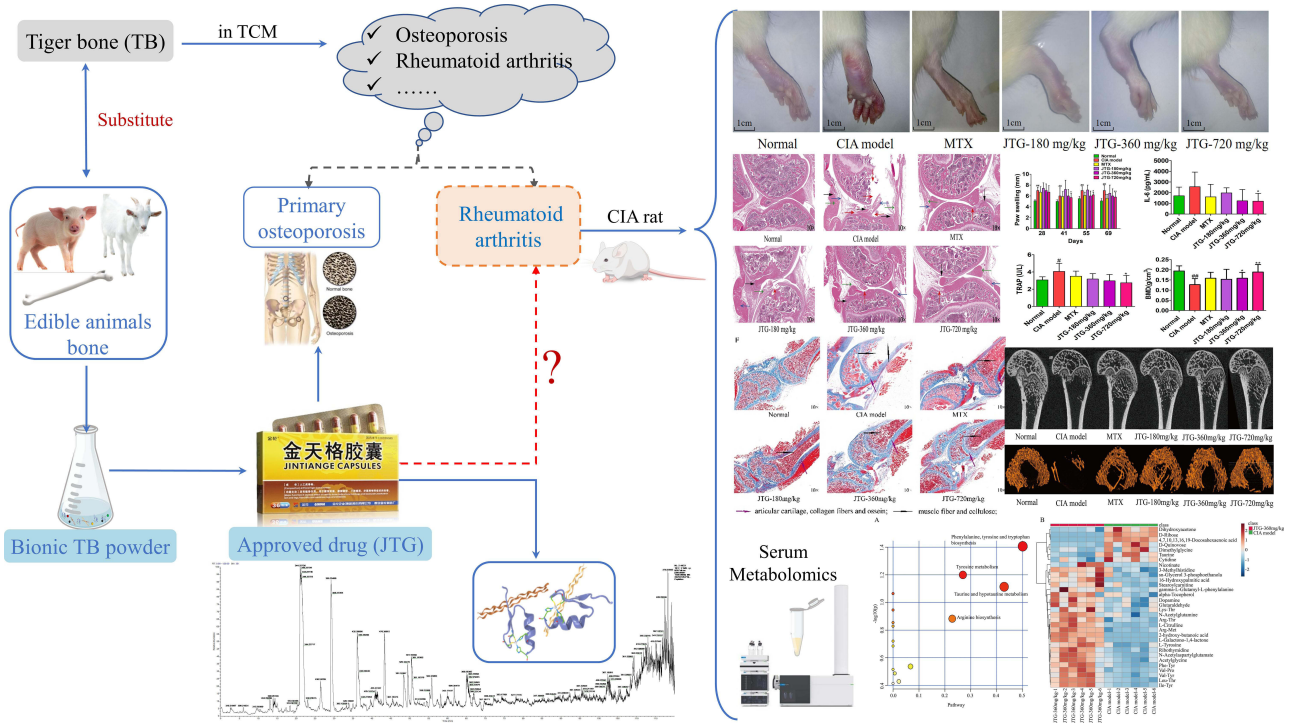


by joint stiffness, hyperplasia, microvascular injury, swelling and pain.[8,9] This leads to reduced quality of life, even to a disability, and increased risk of morbidity and mortality.[10,11] Nevertheless, due to the pathogenetic holism and complexity of the disease, no specific medicine has been able to effectively cure RA so far. Patients with various clinical features of RA were treated with nonsteroidal anti-inflammatory drugs, steroids, disease-modifying anti-rheumatic drugs and immuno-suppressants at present.[12–14] However, side effects such as liver and gastrointestinal disorders limit their extensive clinical application.[15]

Tiger bone (TB) is one of the most precious traditional Chinese medicinal materials, mainly understood and used in TCM to cure osteoporosis, rheumatoid arthritis and bone injury.[16] These pharmaceutical effects of TB were recorded universally in traditional Chinese medicinal classics, such as the best-known Bencao Gangmu (Compendium of Materia Medica).[16] However, given the common concern about tiger conservation, China has banned the domestic trade of TB and its derivatives since 1993 in response to the international tiger trade ban already in place under the Convention on International Trade in Endangered Species of Wild Fauna and Flora (CITES).[17] Hence, pharmacists had to seek effective alternatives, such as TB analogues to eliminate the TB consummation.[18]

Jintiange capsule (JTG) is a formula approved by the Chinese Food and Drug Administration (CFDA) as a TB substitute, which is composed of bionic TB powder with similar ingredients to the natural TB, and rich in bioactive peptides, proteins, amino acids and minerals.[19] That bionic TB powder is prepared from the skeletons of several farmed edible animals including pigs, goats and deer.[19] Ample experimental studies and large clinical trials have demonstrated the prominent efficacies of JTG on alleviating osteoporosis in patients,[19–23] improving the bone microstructure, strengthening the bone biomechanical property in ovariectomized rats,[24] and curing patients with aromatase inhibitor-associated musculoskeletal symptoms.[25] Hence JTG has taken place of TB to treat osteoporosis in clinical for years,[26,27] and been listed as an effective treatment in the guidelines for the treatment of osteoporotic fractures since 2017.[28] However, whether TB substitute JTG could treat RA has been still unclear.

In recent years, metabolomics has been acknowledged to be a powerful tool for identifying potential biomarkers

of RA, which have been reported, such as phenylalanine, tyrosine, taurine, arachidonic acid, histamine, citrulline, and so on.[29–32] Furthermore, applying a systems biology approach using metabolomics can provide a comprehensive functional readout of the organism's physiological status, which is quite suitable for illuminating the therapeutic efficacy and potential mechanism of natural product extracts characterized by multi-component and multi-target.[33]

Inspired by those, we hypothesized that JTG might alleviate RA. Therefore, the aim of the present study was to validate the effect of JTG against RA in CIA rats and use an untargeted metabolomics strategy based on UPLC-Q-TOF/MS to profile the metabolites, with the hope to gain a more comprehensive understanding of the efficacies of the TB substitute JTG and provide experimental evidence for expanding its medicinal application.

# Materials and Methods

## Reagents and Materials

Bovine CII (Chondrex Co., USA) and incomplete Freund's Adjuvant (IFA) (Sigma Co., USA) were used to induce the autoimmune CIA model. Methotrexate (MTX, Xinyi Pharmaceutical Co., Ltd., Shanghai, China) was used as a positive drug to intervene in CIA rats. Serum inflammatory levels of IL-6 and IL-1β levels in CIA rats were detected with Enzyme-linked Immunosorbent Assay (ELISA) kits (Multi Sciences (Lianke) Biotech Co., Ltd., Hangzhou, China). The bone absorption indicators including tartrate-resistant acid phosphatase (TRAP), C-Telopeptide of type I collagen (CTX-I) and RANKL, as well as the bone formation indicators including osteocalcin (OCN) and osteoprotegerin (OPG) were determined in serum by commercial Kits (Nanjing Jian Cheng Bioengineering Institute, Nanjing, China). All the other chemicals and reagents were of analytical-grade purity and purchased from Sinopharm Chemical Reagent Co., Ltd (Shanghai, China).

## Nano-HPLC-MS/MS Analysis of JTG

JTG (National Drug Approval No. Z20030080) in the form of bionic TB power was provided by the drug manufacturer (Ginwa Enterprise Group INC, Co., Ltd., Xi'an, China; Batch No. 210311–1). Due to proteins and peptides being the most important bioactive components in the bionic TB powder JTG,[22,34] JTG was dissolved in ultrapure water and separated by ultrafiltration into two different fractions according to their molecular masses. The peptides of JTG were enriched in a smaller molecular weight distribution below 10,000 Da, while the other distribution with molecular weight above 10,000 Da rich in proteins was digested with trypsin (Promega, Madison, WI) for 24 h at 37°C. Then, nano-HPLC-MS/MS analysis of two fractions was performed on an EASY-nLCTM 1000 system (Thermo Fisher Scientific, Bremen, Germany) connected to a mass spectrometer (Orbitrap Fusion) (Thermo Fisher Scientific, Bremen, Germany) equipped with an online nano-electrospray ion source. Each sample was specifically re-suspended in 40 μL solvent A (A: water with 0.1% formic acid; B: acetonitrile (ACN) with 0.1% formic acid). 2 μL sample was loaded onto the analytical column and subsequently separated with a linear gradient, from 5% B to 30% B in 105 min and 30% B to 90% B in 5 min, remaining there for 2 min; from 90% B to 5% B in 1 min, remaining there for 7 min. The column flow rate was maintained at 300 nL/min. An electrospray voltage of 2.4 kV versus the inlet of the mass spectrometer was used. The Orbitrap Fusion mass spectrometer was operated in a data-dependent mode to switch automatically between Mass Spectrometry (MS) and MS/MS acquisition. Survey full-scan MS spectra (m/z 300–1500) were acquired with a mass resolution of 120 K. The automatic gain control (AGC) target was set to $1x10^5$, and the maximum injection time was 50 ms. Ten sequential high energy collisional dissociation MS/MS scans with a resolution of 15 K were acquired in orbitrap. The intensity threshold was 50,000, and the maximum injection time was 80 ms. The AGC target was set to $1.0x10^5$, and the isolation window was 1.6 Da. Ions with charge states 2+, 3+ and 4+ were fragmented with a normalized collision energy of 30%. The dynamic exclusion time was 10 s for each precursor ion, and then the exclusion time was set to 21 seconds. After detection by HPLC-MS, the original data were taken into the Proteome Discoverer (version 1.3, Thermo Fisher Scientific, Waltham, MA, US), and processed with a mascot server (version 2.3.0, Matrix Science) and the UniProt database. Furthermore, gene ontology enrichment analyses of the biological process and molecular function of the identified JTG proteins and peptides were conducted using the gene ontology database (http://www.geneontology.org/). LC–MS analysis and data mining were processed according to the methods described in the literature.[35,36]

## Animal Treatments

Sixty 7-week-old male Wistar rats weighing (170 ± 10) g (Sippur Will Kay Company) were housed at the Experimental Animal Center of Zhejiang Chinese Medical University (Hangzhou, China, Certificate No. SCXK 2018–0012) and acclimatized for a week under the standard conditions at (24 ± 0.5) °C with 12-hour light–dark cycles, fed standard rodent chow with free access to water. After acclimatization, the 60 rats were equally randomized into 6 groups: a normal and a CIA model group (0.5% CMC-Na sodium 1 mL/100g), a positive control group (MTX 0.05 mg/mL at a 3-day interval), and 3 JTG intervention groups at 180, 360 and 720 mg/kg on alternative days. In the middle-dose JTG-360 mg/kg group, the dose was converted from the drug clinical dose for humans, specifically the daily dose for animals = the daily dose for humans × 6.3/60.[24]

The CIA model was established in Wistar rats according to the reference methods.[37,38] Briefly, bovine CII was dissolved in 0.1 M acetic acid and emulsified in an equal volume of IFA at 4°C to obtain a final CII concentration of 1 mg/mL. In the first day, all rats (except for those in the normal group) were injected with 0.2 mL CII emulsion intradermally as the primary immunostimulation. Secondary immunostimulation was conducted after 20 days to ensure induction of a high incidence of CIA.[39,40] Starting on the day 28, when the CIA model was established, the rats were administered orally with the vehicle, MTX and JTG for 6 weeks. On day 69, all rats were sacrificed by cervical dislocation. The time schedule of the experimental process is illustrated in Figure 1.

All animals were handled according to the National Institute of Health (NIH) guidelines on the ethical use of animals and received humane care. This experiment was approved by the Bioethics Committee of Zhejiang Chinese Medical University (Approval No. IACUC-20200420-04), and the procedures of the experiment were strictly in accordance with the generally accepted international rules and regulations.

## Weight of Body, Spleen and Thymus Measurement

After collecting the serum samples, all rats were sacrificed by cervical dislocation on day 69. The spleen and thymus were immediately removed, washed with saline, and weighed. The spleen index and thymus index of rats, which refer to the ratio of the spleen weight and the thymus weight versus body weight (g/kg), respectively, were calculated for evaluating the extent of influence on immune organs after CII inducing.[41]

## Paw Swelling, Arthritis Score and Inflammatory Mediators Measurement

After the first immunostimulation, the hind paw swelling of rats was measured every 7 days with a Vernier calliper (S·H13050655, Shanghai) independently by two investigators who were blind to the experimental scheme, and the arthritis score was calculated according to the method of Wang et al.[42] The paws were checked and graded for severity and swelling loci by using a 4-point scale: "0", no change; "1", erythema; "2", signs involving the toe and ankle joints with mild swelling; "3", severe swelling involving the entire hind or forepaws and unable to walk. The maximum arthritis score per rat was set at 12 (3 points × 2 fores and 2 hind paws).

In addition, serum Inflammatory factors including IL-1β and IL-6 were detected according to the method described in the ELISA kit instruction manuals. All

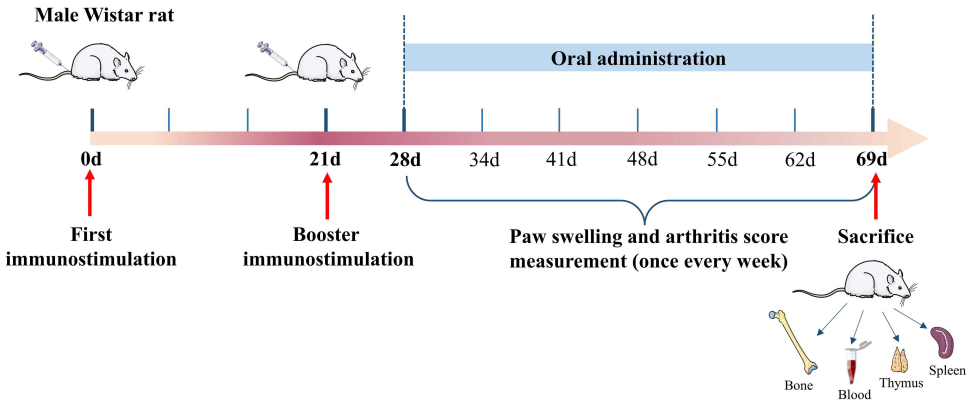


**Figure 1** Schematic of the animal experiment design and process.

reagents and samples must be equilibrated to room temperature before use. The required reaction plate was taken out, and 50 μL of 2-fold diluted standard product and 50 μL serum sample were added to the corresponding reaction plates. Then, 50 μL diluted detect antibody was immediately added to each well. After gent shaking for 30 s, the plate was then incubated at room temperature for 2 h, washed 6 times, added with 100 μL diluted streptavidin-HRP to each well, and incubated again for 45 min at 37°C. The plate was washed again, and added with 100 μL substrate solution, and dark-colored for 30 min, and added with 100 μL stop solution. Finally, the optical density (OD) was measured with a microplate reader (FI-01620 Vantaa, Finland) at 450 nm to draw the standard curve on the ordinate and the standard product curve on the abscissa. The concentration value corresponding to the sample was obtained according to the curve equation.[40]

## Histopathological Observation

The left-hind limbs of the rats were removed postmortem, the isolated femur bone was fixed in 4% paraformaldehyde for more than 24 h, decalcified with 4% EDTA for a month at 4°C, paraffin-embedded, and sliced into 4 μm sections. The sections were deparaffinized, routinely stained with HE[37,40] and Masson,[43] further observed under a panoramic scanner (Pannoramic MIDI, Hungary).

## Serum Bio-Marker Related to Bone Metabolism Measurement

Rat blood samples were obtained from the abdominal main artery and solidified at room temperature for 2 h to collect the serum. Serum bio-markers related to bone absorption including TRAP, CTX-I and RANKL, as well as to bone formation including OCN and OPG were measured according to the instruction manual of the ELISA kit. All reagents and samples must be equilibrated to room temperature before use. The required reaction plate was taken out, and 50 μL 2-fold diluted standard product and 50 μL serum sample were added to the corresponding reaction plates. Then, 50 μL diluted detect antibody was immediately added to each well. After gent shaking for 30 s, the plate was incubated at room temperature for 1 h, washed for 5 times, added with 50 μL diluted streptavidin-HRP to each well, and incubated again for 1 h at 37°C. Subsequently, the plate was washed again, added with 50 μL chromogenic solution A and B, respectively, and dark-colored for 10 min, added with 50 μL stop solution, and read for OD on a microplate reader (FI-01620 Vantaa, Finland) at 450 nm. According to the OD value, the standard curve was drawn on the ordinate and the standard product was drawn on the abscissa. The concentration value corresponding to the sample was obtained according to the curve equation.[40]

## Micro-CT Analysis and Bone Tissue Observation

The trabecular micro-architecture of the rat right femur was measured on a micro-CT system (Sky Scan 1172) under the following conditions: the tube current at 112 μA, peak voltage at 80 kV, scanning resolution ratio at 9 μm per pixel, exposure time at 370 ms, angular rotation at 360°, increment at 0.6°, frame average at 2, and the image resolution ratio at 17.81 μm. The obtained images were imported into the Micview V2.1.2 software for 3D reconstruction. Parameter correction was based on a specific scanning protocol.[33] After 3D reconstruction of the bone images, the morphometric parameters were measured using Advanced Bone Analysis software.

Bone mineral density (BMD, mg/cc) was calculated from the CT attenuation values by means of a calibration phantom scanned with the animal.[44] The microarchitectural characteristics of the trabecular bone were investigated by examining 2D sections of the bone biopsies, combined with calculation of morphometric parameters using 3D methods.[45] The basic morphometric indices included measurement of the bone volume (BV) and the total volume of interest (TV), which can be derived from either a simple voxel-counting method or a more advanced volume-rendering method, which is also referred to as volumetric marching cubes.[46] The ratio of these two measurements was termed as bone volume fraction (BV/TV or BVF; %). Moreover, bone surface (BS) was computed by triangulation of the object surface using a marching-cubes algorithm. Then, bone surface (BS/BV; 1/U) was derived from those indicators.[47] Trabecular number (Tb.N; 1/mm), trabecular thickness (Tb.Th; mm) and trabecular separation (Tb.Sp; mm) were based on 3D calculations, a sphere-fitting method. The spheres were fitted to the object and background to measure the Tb.Th and Tb.Sp, respectively.[48] Tb.N was calculated as the inverse of the mean distance between the mid-axes of the structure, which were derived via the distance-transformation method.[49]

## Metabolomics Analysis

Rat serum samples (100 μL) were mixed with 400 μL extract solution (acetonitrile: methanol=1:1) containing internal standard (L-2-Chlorophenylalanine, 2 μg/mL), which was applied to improve the data quality and check the autonomous integration success of the software. Then, the mixture was incubated at −40°C for 1 h before being centrifuged (10,000 rpm) at 4°C for 15 min to denature the serum proteins. Then, the supernatant was filtered through 0.22 μm stainless-steel filters and transferred into autosampler vials for further analysis. A total of 30 analytical samples from the five groups were analyzed. In addition, the quality control (QC) sample was prepared by taking 10 μL from each 30 samples, respectively, then analyzed after every four injections to monitor the system stability of analysis.[50]

The samples were analyzed by UPLC-Q-TOF-MS (Agilent 1290 Infinity LC system and Agilent 6538 UHD Accurate-mass Q-TOF spectrometer, Agilent Technologies, Santa Clara, CA, USA) with UPLC BEH Amide column (2.1 × 100 mm, 1.7 μm; Waters, Milford, MA, USA). The mobile phase consisted of 25 mmol/L ammonium acetate and 25 mmol/L ammonia hydroxide in water (pH = 9.75) (A) and ACN (B). The gradient elution program was as follows: 95% B at 0–0.5 min, 95–65% B at 0.5–7.0 min, 65–40% B at 7.0–8.0 min, 40% B at 8.0–9.0 min, 40–95% B at 9.0–9.1 min, 95% B at 9.1–12.0 min, with a flow rate of 0.4 mL/min. The temperature of the column was 25°C, and the autosampler 4°C. The injection volume was 2 μL. Triple TOF 6600 mass spectrometry was used to acquire MS/MS spectra on an information-dependent basis during an LC/MS experiment. In this mode, the acquisition software (Analyst TF 1.7, AB Sciex) continuously evaluated the full scan survey MS data. It collected and triggered the acquisition of MS/MS spectra depending on the preselected criteria. In each cycle, the most intensive 12 precursor ions with intensity above 100 were chosen for MS/MS at a collision energy of 30 eV. The cycle time was 0.56 s. ESI source conditions were set as follows: Gas 1 as 60 psi, Gas 2 as 60 psi, Curtain Gas as 35 psi, Source Temperature as 600°C, Declustering potential as 60 V, Ion Spray Voltage Floating as 5000 V or −4000 V in positive or negative modes, respectively.

## Data Processing and Multivariate Data Analysis

Nonparametric data were compared using Mann–Whitney *U*-test, and parametric data were compared using one-way analysis of variance (ANOVA) followed by Least Significance Difference's (LSD) multiple comparison post hoc test. All data analyses were completed using GraphPad Prism version 5.0 software and Statistical Product and Service Solutions (SPSS) version 22.0 software. The *P* values <0.05 were considered to be statistically significant.

Tandem mass spectra of nano-HPLC-MS/MS analysis of JTG were extracted by PEAKS Online software (X Build, version 1.4.2020–10-02_113407). MS spectra lists were searched against their homologous species level UniProt FASTA databases (https://www.uniprot.org/) assuming the nonspecific digestion. PEAKS were searched with a fragment ion mass tolerance of 0.020 Da and a parent ion tolerance of 10.0 PPM. The variable modifications were specified as Oxidation of methionine. Peptide and protein confidence (−10 logp) was set to 20.

MS raw data (.wiff) of metabolomics analysis was transformed into a common data format (.mzdata) by using ProteoWizard software and processed by R package XCMS (version 3.2) for peak deconvolution alignment and integration. After mean-centering and Pareto-scaling procedures, the resultant data matrices were introduced to the SIMCA (V14.1, Sartorius Stedim Data Analytics AB, Umea, Sweden) for principal component analysis (PCA) and orthogonal projections to latent structures discriminant analysis (OPLS-DA). The value of variable importance in projection (VIP), which reflects the importance of detected metabolites, was calculated using SIMCA software.[51] Further, VIP values (VIP > 1) and *t*-test ($P < 0.05$) were introduced as two limited conditions to wash data for screening the potential biomarkers. Afterwards, biochemical databases including Human Metabolome Database (HMDB, http://www.hmdb.ca/) and PubChem (http://www.ncbi.nlm.nih.gov/pccompound/) were used to identify metabolites. MetaboAnalyst 5.0 (http://www.metaboanalyst.ca/) was used for pathway analysis to interpret metabolites, meanwhile for visual heat map analysis to reflect changes in each metabolite.

# Results

## Peptide and Protein in JTG

The total ions chromatography (TIC) of proteins and peptides in JTG by nano-HPLC-MS/MS analysis are shown in Figure 2. Further, the raw data of MS spectra were imported into the Proteome Discoverer (version 1.3, Thermo Fisher Scientific, Waltham, MA, United States) for filtration. The collected data files were processed and sent to a MASCOT server (Version 2.3.0, Matrix Science)

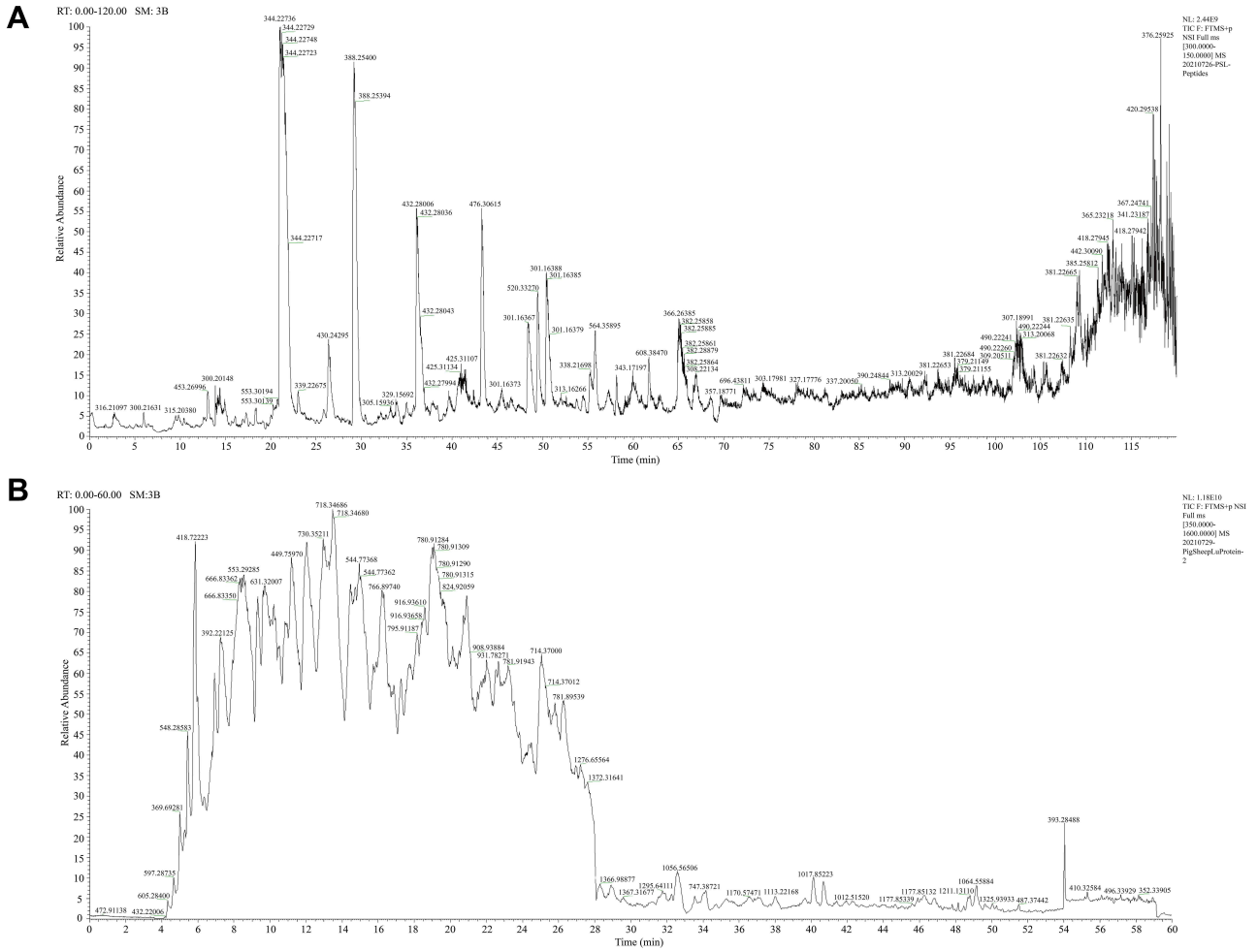


**Figure 2** The total ions chromatography of JTG. (**A**) Peptide fraction; (**B**) protein fraction.

for proteins and peptides identification by using the UniProt database (http://www.uniprot.org/) with the taxonomy constraint of Sus scrofa (Pig, taxonomy/9823, reviewed entries 1438, 2021-07-23), Caprinae (goat, taxonomy/9963, reviewed entries 637, 2021-07-23) and Cervidae (deer, taxonomy/9850, reviewed entries 149, 2021-07-23). As results, 9 bioactive peptides (Table 1) were identified straightly from the peptide fraction of JTG through peptidomics analysis, and 348 proteins (Table S1) were determined from trypsin digested protein fraction of JTG through proteomics analysis of MASCOT search. These identified proteins and peptides were annotated based on the GO database (http://www.geneontology.org/), and further function enrichment analysis (GO annotation) results implied that bioactive peptides of JTG may possess molecular functions of microfilament motor activity, motor activity, ATPase activity, actin binding and ATP binding (Figure 3A), thus might be involved in biological process of striated muscle contraction, muscle contraction, response to hydrogen peroxide and response to mechanical stimulus (Figure 3B). Besides, proteins of JTG may possess molecular functions of protein binding, enzyme binding, identical protein binding, ubiquitin protein ligase binding, calcium ion binding, protein homodimerization activity, ATP binding and protein heterodimerization activity (Figure 3C), thus, might be involved in biological process of response to drug, aging, positive regulation of gene expression, negative regulation of the apoptotic process, the oxidation-reduction process, positive regulation of cell proliferation, positive regulation of transcription, DNA-templated and positive regulation of transcription from RNA polymerase II promoter (Figure 3D).

## JTG Affects Body Weight, Spleen and Thymus in CIA Rats

According to the last measurement on day 69, the body weight of rats in the normal group was (380.5±16.9) g and

**Table 1** Bioactive Peptides Identified from JTG

| No. | Peptide | Mass | Length | m/z | RT | Accession |
|---|---|---|---|---|---|---|
| 1 | PSGPQTP | 682.3286 | 7 | 683.3365 | 0.049 | P21692\|MMP1_PIG |
| 2 | GPAGDARVP | 838.4297 | 9 | 420.2223 | 1.0986 | Q29400\|IBP2_SHEEP |
| 3 | HGCLLLSPGN | 1009.5015 | 10 | 505.7546 | 2.0037 | Q5MNU5\|SCAP_PIG |
| 4 | AGPAGDARVP | 909.4668 | 10 | 455.7408 | 4.2283 | Q29400\|IBP2_SHEEP |
| 5 | VKAHGQ(+0.98)KVADAL | 1236.6826 | 12 | 619.3491 | 6.0053 | P01965\|HBA_PIG |
| 6 | GEKVAN(+0.98)AL | 801.4232 | 8 | 401.7187 | 12.5431 | P21379\|HBA_RANTA; P01971\| HBA_ALCAA |
| 7 | VGN(+0.98)HSAGSAVGPEAAGAPVPMQ (+0.98)GEAPQ | 2487.1335 | 27 | 830.0527 | 16.886 | Q9XT50\|ATP7B_SHEEP |
| 8 | PASTPPAAPA | 878.4498 | 10 | 440.2324 | 23.7267 | Q9TU17\|CXA3_SHEEP |
| 9 | AAALRKKH | 893.5559 | 8 | 447.7883 | 29.1562 | Q9TV63\|MYH2_PIG; P79293\| MYH7_PIG; Q9TV62\|MYH4_PIG |

in CIA model group was (348.1±25.8) g, which reflected a significant lower body weight change compared with normal rats (Figure 4A). Nevertheless, the body weight loss in CIA model rats was alleviated mildly in rats administered with JTG, for example, the body weight of rats in the group of JTG-720 mg/kg was (357.1±18.3) g.

As a result, there were no significant changes in the spleen index in groups (Figure 4B). It represented spleen as immune organ might be less influenced after CII stimulation. Nevertheless, it might have more influence on the other immune organs of thymus, since the thymus index of the CIA rats was significantly decreased from (1.21±0.31) g/kg to (0.90±0.10) g/kg compared with normal rats, and revised dramatically in rats administered with JTG both in doses of 180 mg/kg and 720 mg/kg (Figure 4C).

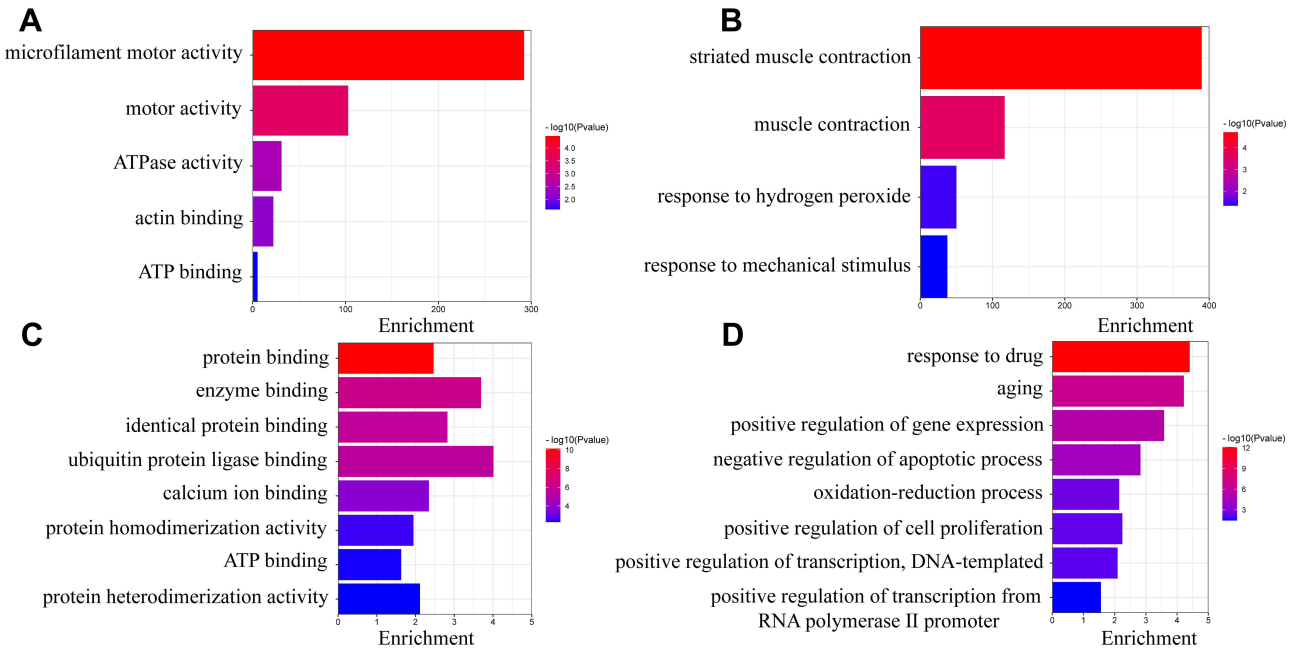


**Figure 3** Bioinformatic analysis of the constituents in JTG: Molecular functions of peptides (**A**) and proteins (**B**); Biological process of peptides (**C**) and proteins (**D**).

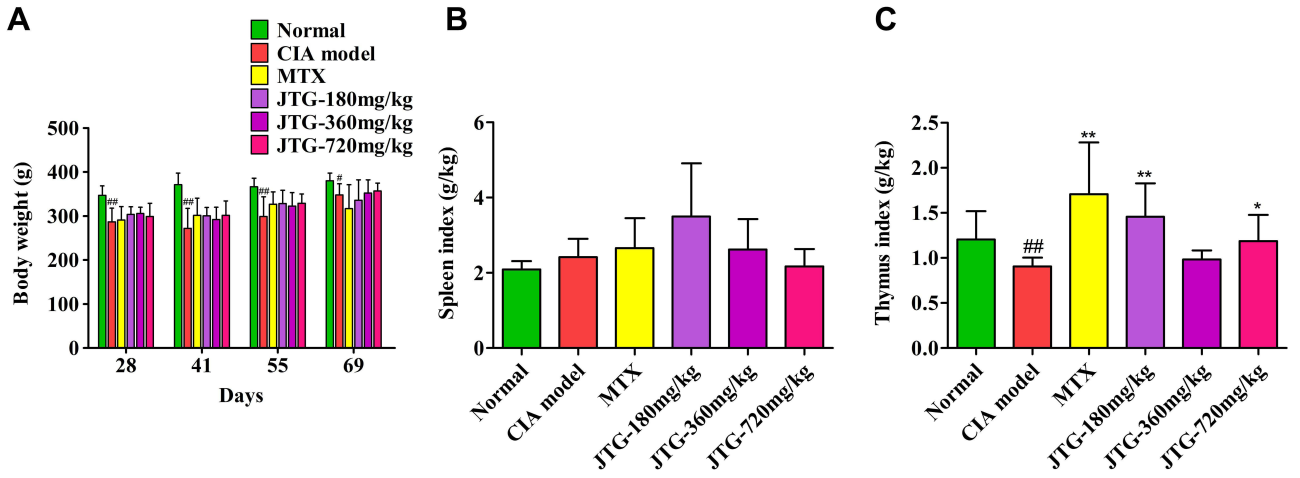


**Figure 4** Effects of JTG on body weight, spleen and thymus in CIA rats. (**A**) Body weight; (**B**) Spleen index; (**C**) Thymus index. Data were expressed as the mean ± SD (n=10), $^{\#}P < 0.05$, $^{\#\#}P < 0.01$ vs normal group; $^{*}P < 0.05$, $^{**}P < 0.01$ vs CIA model group.

## JTG Alleviates Paw Swelling and Arthritis in CIA Rats

During the animal experiment, there were no obvious symptoms of immune responses after primary immunostimulation in the early stage. Compared with normal group, the rats in the model group developed caudal root ulcer, paw swelling, dry hair, alopecia, decreased activity, decreased appetite, and more aggressiveness after the booster immunostimulation. Symptoms of arthritis in most rats of the model group gradually became worse than represented by acute articular inflammation, hyperemia, pink and shiny skin surface, inability to bear weight, limited movement, and red and swollen front paws. Moreover, some rats were unable to move basically. Arthritis of rats was symmetrical, and the symptoms were more serious in the hind limbs. The pathological phenotype changes in CIA rats reversed significantly after intervention with the test drug (Figure 5A). Paw swelling was used as the determinant of the severity of arthritis. As expected, the hind paw volume was obviously increased after CIA immunostimulation. However, MTX showed significant potency in inhibiting the paw swelling of the CIA rats (Figure 5B). Similarly, JTG administration (360 and 720 mg/kg) dramatically mitigated paw edema compared with the rats in CIA model group. In addition, the arthritis scores in the CIA rats were decreased significantly after MTX or JTG treatment at the dose of 360 and 720 mg/kg (Figure 5C). The arthritis scores correspond to the paw swelling levels of the rats.

## JTG Down-Regulates Serum Pro-Inflammatory Cytokines Levels in CIA Rats

Pro-inflammatory cytokines are known to play vital roles in maintaining chronic inflammation and tissue damage during RA progression. The serum levels of pro-inflammatory cytokines IL-1β and IL-6 were measured to assess the severity of arthritis using ELISA kits. The results showed that the serum levels of IL-6 (Figure 5D) and IL-1β (Figure 5E) in the CIA model rats were augmented compared to those in the normal rats. However, the serum levels of IL-1β were down-regulated after MTX and JTG intervention in both 360 and 720 mg/kg dose groups, and the serum levels of IL-6 were significantly decreased in three JTG groups especially in 720 mg/kg ($P<0.05$) compared with that in the CIA model group. The above results demonstrated that JTG had an immunomodulatory effect in CIA rats.

## JTG Reverses Ankle Joint Histopathological Change in CIA Rats

The therapeutic effect of JTG on CIA rats was further confirmed by histopathological analysis of the ankle joint. Massive mononuclear cell infiltration of the synovial tissue and synovial hyperplasia, pannus formation, cartilage hyperplasia and erosion were observed in the ankle joint of the CIA rats, and these symptoms were reduced significantly in CIA rats treated with MTX or JTG compared with the model control CIA rats. These results indicated that JTG at doses of 180, 360 and 720 mg/kg

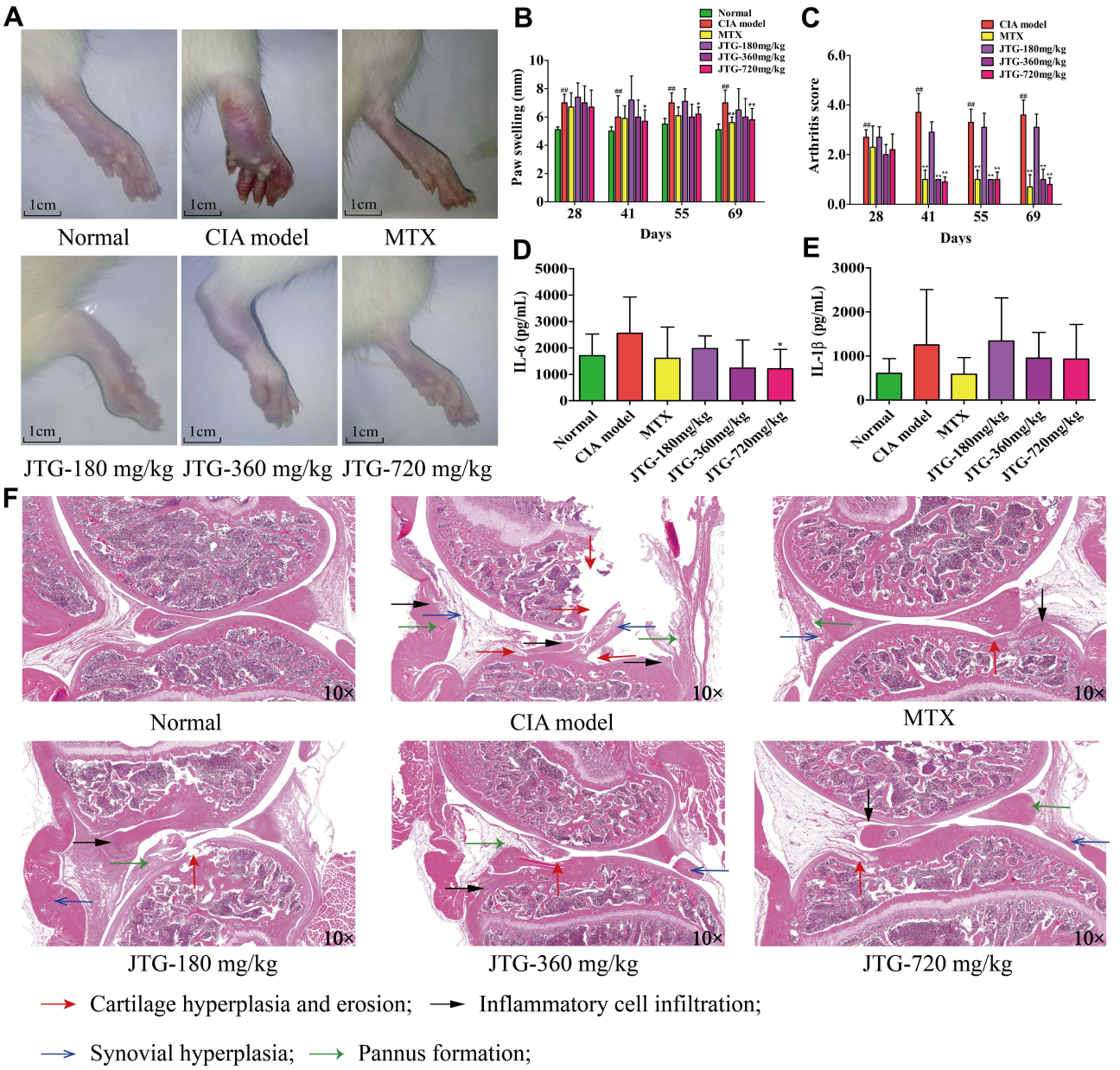


**Figure 5** Effects of JTG on rheumatoid arthritis in CIA rats. (**A**) Pathological phenotype changes in CIA rats; (**B**) Paw swelling; (**C**) Arthritis score; (**D**) Serum IL-6 level; (**E**) Serum IL-1β level; (**F**) Histopathological changes of joints in CIA rats treated with JTG. The red arrow indicates cartilage hyperplasia and erosion; the black arrow indicates inflammatory cell infiltration; the blue arrow indicates the synovial hyperplasia; the green arrow indicates pannus formation. Data were expressed as the mean ± SD (n=10), $^{\#\#}P < 0.01$ vs normal group; $^{*}P < 0.05$, $^{**}P < 0.01$ vs CIA model group.

could successfully alleviate the arthritic symptoms induced by CII (Figure 5F).

## JTG Regulates Bone Metabolism-Related Serum Biochemical Markers in CIA Rat

Bone metabolism-related biochemical parameters were detected using ELISA kits. The serum levels of biomarkers related to bone resorption include TRAP, RANKL and CTX-I. Serum TRAP (Figure 6A) was observably enhanced in the CIA rats compared with normal rats ($P<0.05$), and significantly reduced after treatment with JTG-720 mg/kg ($P<0.05$). RANKL (Figure 6B) remained unchanged significantly in all groups. CTX-I (Figure 6C) was significantly increased in the CIA model rats compared with normal rats ($P<0.05$), while it was not significantly changed after treatment with all three JTG groups. Nonetheless, the serum OCN (Figure 6D), an indicator of bone formation, was increased in the CIA rats compared with that in the normal rats at the end of the 6-week treatment, while the treatment with JTG significantly

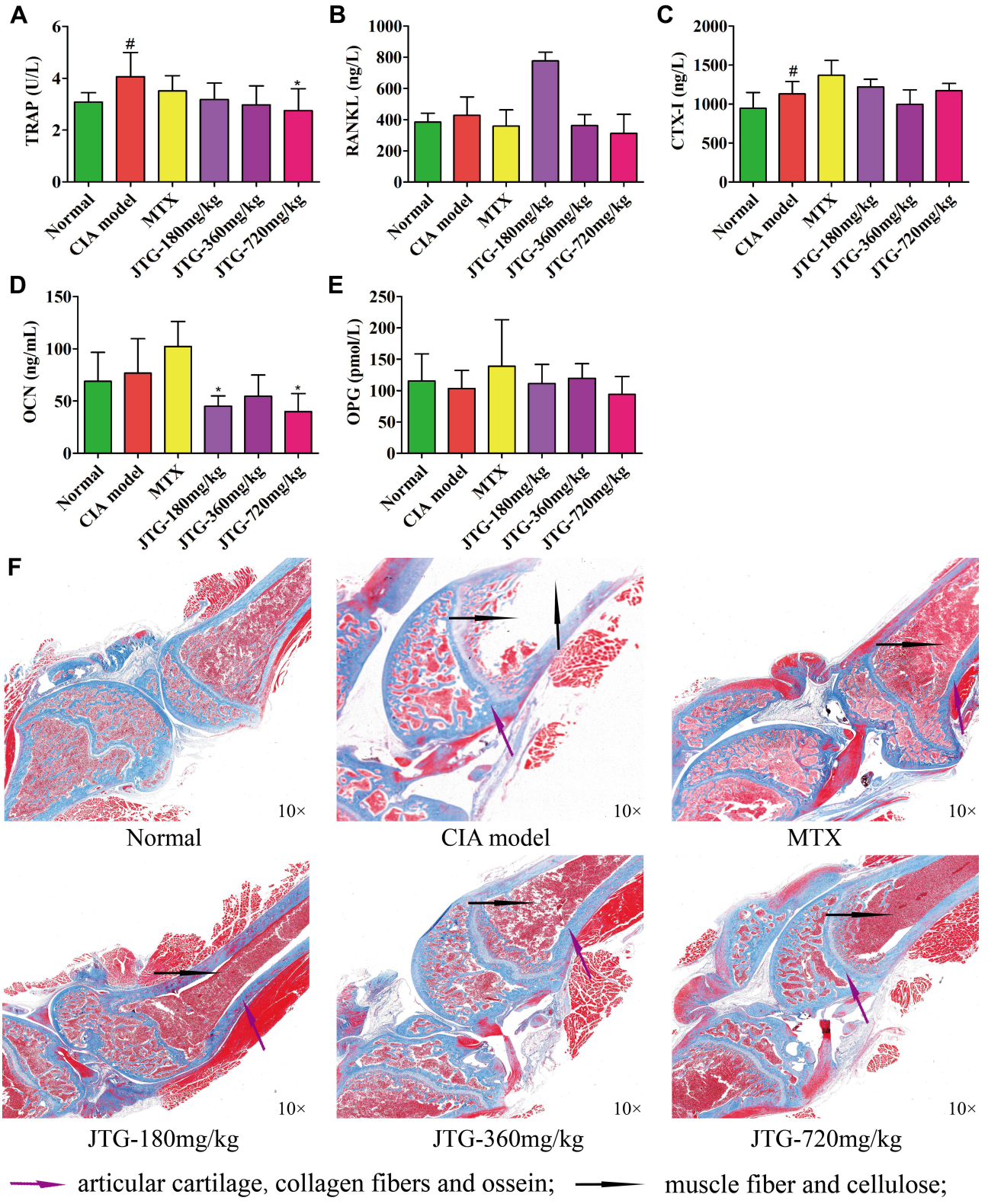


**Figure 6** Effects of JTG on bone metabolism-related biochemical factors, bone tissue injury, bone morphology and bone micro-architecture in CIA rats. (**A**) Serum TRAP; (**B**) Serum RANKL; (**C**) Serum CTX-I; (**D**) Serum OCN; (**E**) Serum OPG; (**F**) Histopathological analysis of the bone tissue sections with Masson staining in CIA rats. The black arrow indicates articular cartilage, collagen and ossein; the purple arrow indicates muscle fiber and cellulose. Data were expressed as mean ± SD (n=10), $^{\#}P < 0.05$ vs normal group; $^{*}P < 0.05$ vs CIA model group.

reduced the OCN level in CIA rats ($P<0.05$). Serum OPG (Figure 6E) remained unchanged significantly in all groups.

## JTG Relieves Bone Tissue Injury in CIA Rats

Histopathological analysis of the bone tissue sections with Masson staining was also induced to further confirm the therapeutic effect of JTG on CIA rats. As shown in Figure 6F, the articular cartilage containing collagen fibers and ossein was dyed in blue. In contrast, the bone trabecula in the bone marrow cavity was dyed in red since its surface was covered with a layer of osteogenic cells and osteoblasts, which secreted organic matrix and fibers. In the normal rats, the subchondral bone matrix and bone trabecula in the bone marrow cavity were dense. At the same time, the content of bone trabecula was significantly reduced, and the cartilage was also destroyed in the CIA model rats. Nevertheless, such bone tissue injury was significantly relieved in rats administered with MTX or JTG.

## JTG Improves Bone Morphology and Bone Micro-Architecture in CIA Rats

BMD was significantly decreased ($P<0.01$) in CIA rats as compared with that in the normal rats, while notably increased in JTG-360 mg/kg ($P<0.05$) and JTG-720 mg/kg ($P<0.01$) treated CIA rats as compared with that in the model rats (Figure 7A). Further analysis of the bone structural properties revealed that the trabecular bone microarchitecture in the CIA rats were significantly decreased in BVF (Figure 7B), Tb.Th (Figure 7D), and Tb.N (Figure 7E), and had significantly increased in BS/BV (Figure 7C) and Tb.Sp (Figure 7F). As a result, after being treated with 720 mg/kg JTG, the BVF and Tb.N were increased dramatically ($P<0.05$), while Tb.Sp and BS/BV decreased significantly ($P<0.01$).

Arthritis is known to be associated with an increase in trabecular bone loss in the metaphyseal region of distal femur. Representative 2D (Figure 7G) images can directly obtain BV/TV, and direct 3D (Figure 7H) measurement of trabecular morphology, such as Tb.Th, Tb.N and Tb.Sp, rather than inferring these values based on 2D stereologic models.[52] JTG showed the protective effect on trabecular structure in cancellous bone of distal femora in CIA model rats. This change could be demonstrated by lower BVF (Figure 7B) in the trabecular bone of distal femur in CIA rats (Figure 7G). In addition, the 3D trabecular bone structure of the distal femur was destroyed obviously in CIA rats (Figure 7H) in terms of Tb.Th (Figure 7D), Tb.N (Figure 7E) and Tb.Sp (Figure 7F). The above findings indicate that arthritis had an especially strong deteriorating effect on the peri-articular bone adjacent to the inflamed joints, and JTG could reverse this deterioration, especially alleviate the femoral bone loss and improve the trabecular bone microstructure.

## Metabonomics Insights

The total ions chromatography (TIC) of serum samples of CIA model rat (Figure S1) and Quality control (QC) samples (Figure S2) are shown in the Supplementary materials. Multivariate analysis was performed to investigate metabolic differences between groups.

The QC sample was injected regularly (every four samples) throughout the entire running process to monitor the system stability. The results showed that the LC-MS analysis was stable and reliable.

The cumulative interpretation rate of the PCA in the positive ion mode was $R^2X = 0.607$, $Q^2 = 0.285$, and the PCA in the negative ion mode was $R^2X = 0.644$, $Q^2 = 0.284$. In Figure 8, the cross-coordinate Principal component 1 (PC1) and the ordinate PC2 indicate the score of the first and second principal components, respectively. The percentage of explained variance of the PCA for PC1 and PC2, respectively, was 20.6% and 11.5% in the positive ion mode (Figure 8A) and 20.3% and 14.3% in the negative ion mode (Figure 8B), respectively. The results in Figure 8 showed that the samples of CIA model group could be significantly separated from those of normal group, suggesting that metabolic changes occurred in CIA rats. After JTG administration, the samples of JTG groups in 360 mg/kg and 720 mg/kg dose were approximately separated from those of CIA model group. The above results suggested that JTG could reverse changes in serum metabolic profile in CIA rats. Because the dose of JTG 360 mg/kg for animals was converted from the clinical drug dose for humans, the following data of metabolomics analysis were mainly displayed with samples of JTG group in 360 mg/kg dose. These PCA figures show the distribution of the original data, indicating that the three JTG dose groups and the model group were clearly separated from the normal control group. These results showed good stability of the whole method and high data quality.

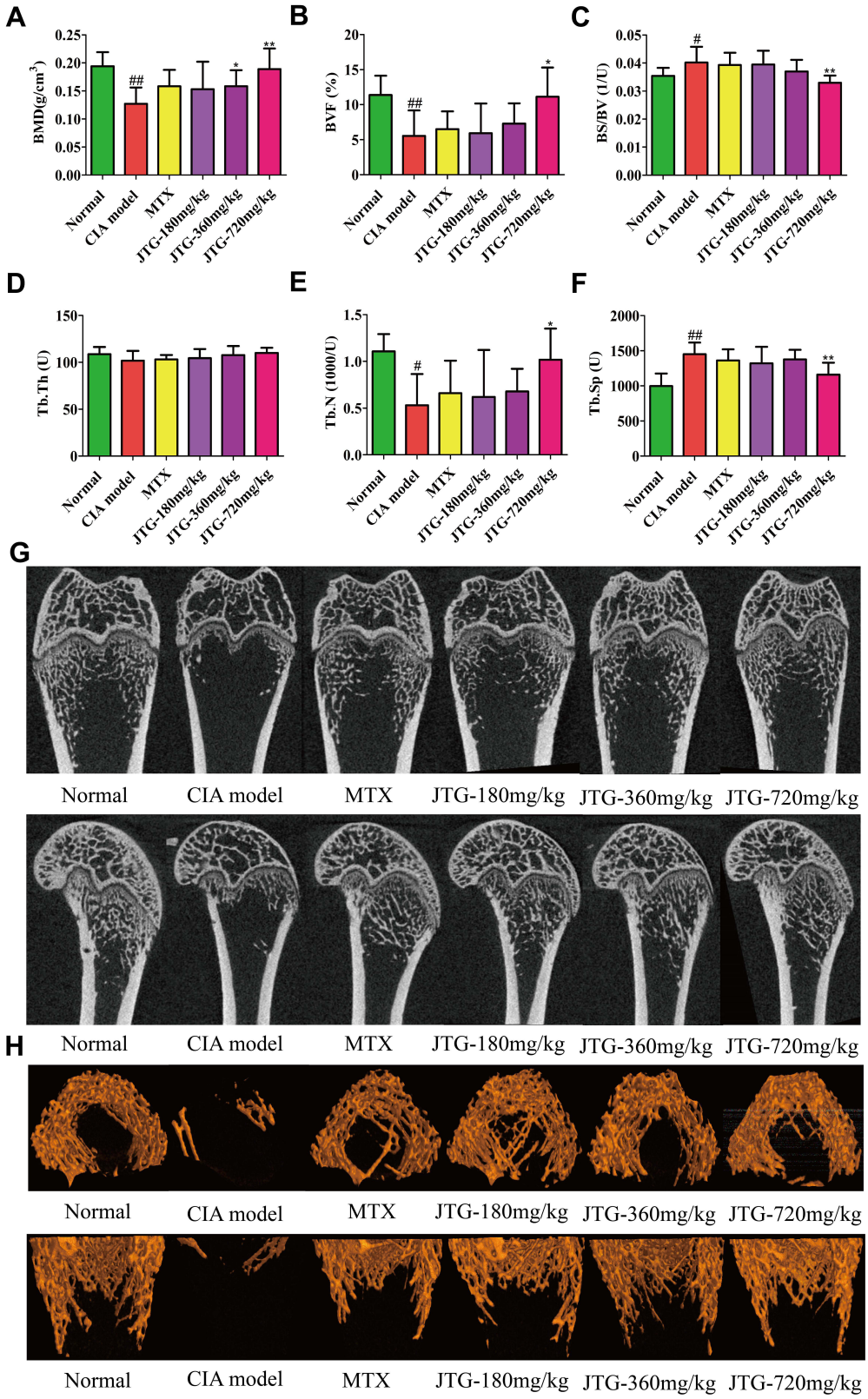


**Figure 7** Effects of JTG on bone morphology and bone micro-architecture in CIA rats. (**A**) BMD; (**B**) BVF; (**C**) BS/BV; (**D**) Tb.Th; (**E**) Tb.N; (**F**) Tb.Sp; (**G**) 2D scanning images of the rat femur (can observe the density of bone trabecular); (**H**) 3D scanning images of the rat femur (can more intuitively observe the structure, density and morphology of bone trabecular.) Data were expressed as the mean ± SD (n=10), $^{\#}P < 0.05$, $^{\#\#}P < 0.01$ vs normal group; $^{*}P < 0.05$, $^{**}P < 0.01$ vs CIA model group.

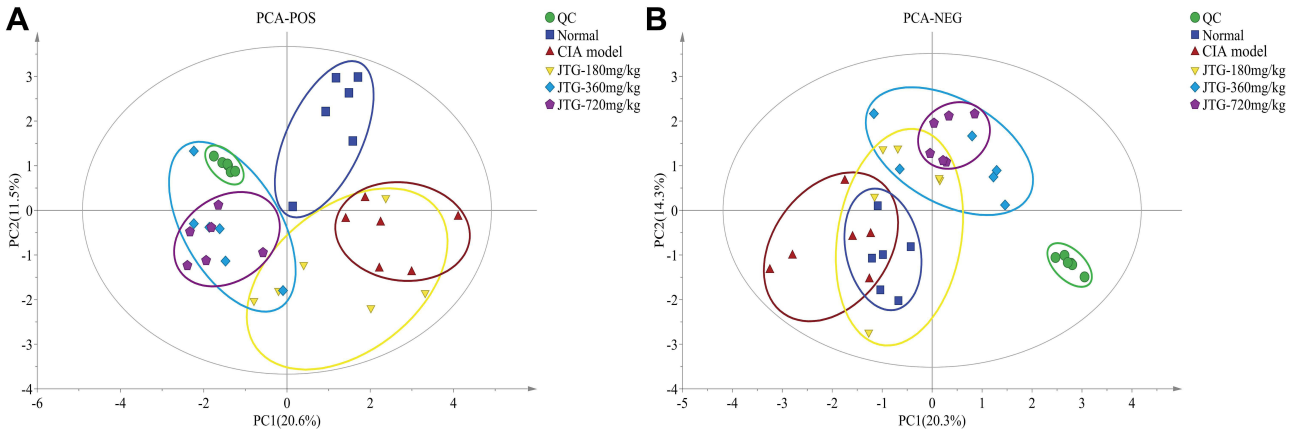


**Figure 8** PCA score plot shows preliminary separation between serum samples and QC. (**A**) Positive ion mode; (**B**) negative ion mode.

## Identification of Potential Biomarkers in CIA Rat

To gain a better understanding of the variables responsible for classification, OPLS-DA was supervised in both positive and negative ion modes. After 200 permutations,[53,54] the intercept value of $R^2Y$ and $Q^2Y$ was 0.905 and −0.159, respectively (Figure 9A). The value of $R^2Y$ was close to 1, indicating that the established model conformed to the true situation of sample data. The negative value of $Q^2Y$ intercept indicated the robustness of the model, showing a low risk of overfitting and reliability. The OPLS-DA score plot between normal and model groups in the positive ion mode (Figure 9B) was further shown. The S-plot was employed to identify altered metabolites that markedly contributed to the differences between the normal and model groups (Figure 9C). The value of p[1] indicated the impact of X variable on the group, and the p(corr)[1] indicated the reliability of the impact of X variables. Therefore, the metabolites in the lower left corner and upper right corner of S-plot were critical. In brief, based on the distribution trend of metabolites, we could further confirm that the CIA model was set up successfully.

To further confirm the significant variables, the first principal component of VIP was calculated, and VIP value >1 and $P < 0.05$ of Student's *t*-test were considered

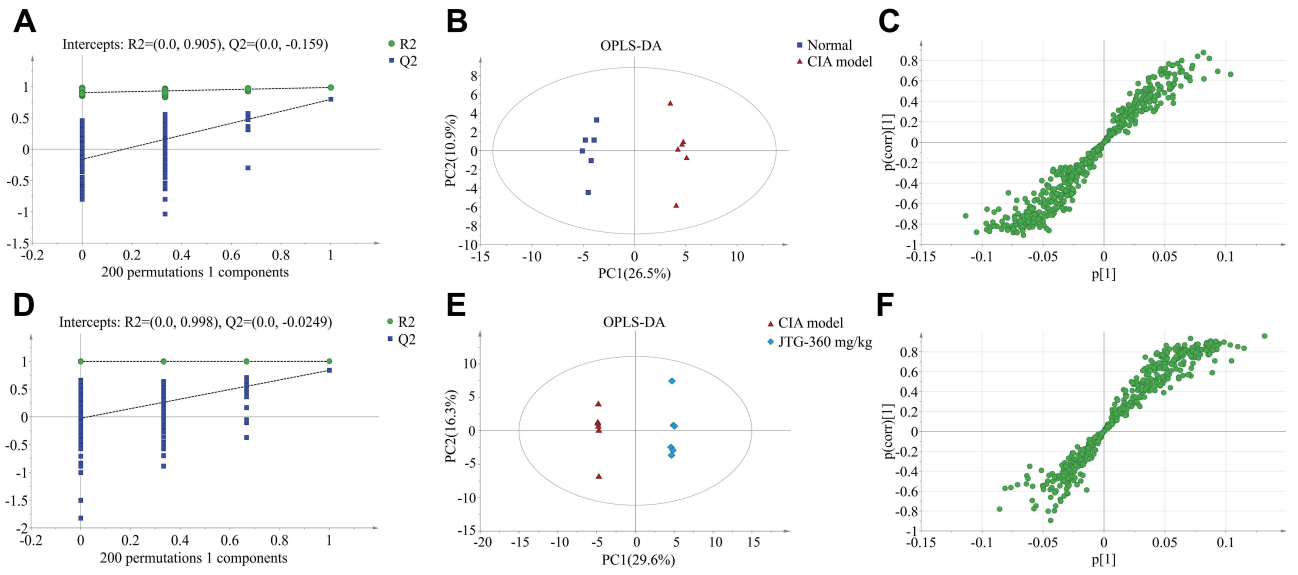


**Figure 9** The analysis of UHPLC-Q/TOF-MS of serum samples of CIA rats. Statistical validation of the orthogonal partial least square discriminant analysis (OPLS-DA) model in 200 random permutation tests. Green dots are the $R^2$ values and blue blocks are the $Q^2$ values. Between normal and CIA model groups: (**A**) validation of OPLS-DA model in positive ion mode; (**B**) OPLS-DA score plot in positive ion mode; (**C**) an S-plot of the normal and CIA model groups. Between CIA model and JTG-360 mg/kg groups: (**D**) validation of OPLS-DA CIA model in positive ion mode; (**E**) OPLS-DA score plot in positive ion mode; (**F**) an S-plot of the CIA model and JTG-360 mg/kg groups.

as statistical difference. As a result, 38 differential metabolites between the normal and CIA model rats were selected as potential biomarkers. Furthermore, the results of MetaboAnalyst 5.0 pathway analysis (impact >0.1) showed that the potential biomarkers were mainly involved in the critical pathways, including: 1) Phenylalanine, tyrosine and tryptophan biosynthesis; 2) Taurine and hypotaurine metabolism; 3) Arachidonic acid metabolism; 4) Tyrosine metabolism; 5). Arginine biosynthesis; 6) Histidine metabolism (Figure S3).

## JTG Reverses Changes of Serum Metabolic Profile in CIA Rats

To investigate the impact of JTG on the serum metabolic profiles in CIA rats, OPLS-DA scores plot was built to depict the general variation between the normal control and model groups after JTG intervention. Serum metabolic changes in CIA rats in the three JTG dose groups were observed. After 200 permutations, the parameters of OPLS-DA analysis between the model and 360 mg/kg JTG dose groups were $R^2Y = 0.998$ and $Q^2Y = -0.0249$ in positive ion mode (Figure 9D), and the results with 180 mg/kg and 720 mg/kg JTG dose groups are shown in Figure S4A and Figure S5A, respectively. The score plots in the positive ion mode of the three JTG dose groups were completely separated from the model group. The results with 360 mg/kg JTG dose group are shown in Figure 9E-F and those with 180 mg/kg and 720 mg/kg are shown in Figure S4B and C and Figure S5B and C. All these results indicated that the serum metabolic pattern underwent significant changes in JTG groups compared with model group. Furthermore, 32 differential metabolites were identified by comparison between the CIA model group and JTG group in 360 mg/kg dose (Table 2), while 13 and 30 differential metabolites were identified by comparing between the CIA model group and JTG group in 180 mg/kg dose and 720 mg/kg dose (Table S2).

Furthermore, the results of MetaboAnalyst 5.0 pathway analysis (impact >0.1) hinted the potential significant pathways.[55] It implied that the potential pathways related to JTG (360 mg/kg) intervention in CIA rats were the biosynthesis pathways of phenylalanine, tyrosine, and tryptophan ($P < 0.05$), and the metabolism pathways of taurine, hypotaurine and tyrosine, moreover the biosynthesis pathway of arginine (Figure 10A). In addition, the visual heat map intuitively reflected each metabolic change in each rat sample. As shown in the heat map, the levels of serum biomarkers in rats administered with JTG in 360 mg/kg dose (Figure 10B) have been remarkably revised compared with those in CIA model rats. In addition, the bubble diagrams of the potential pathways related to JTG intervention (180 mg/kg in Fig. S4D; 720 mg/kg in Fig. S5D) in CIA rats and the heat maps reflecting each metabolic change of JTG intervention (180 mg/kg in Figure S4E; 720 mg/kg in Figure S5E) in CIA rats were displayed in supplementary materials.

# Discussion

Rheumatoid arthritis, as a systemic inflammatory disease, is characterized as the clinical manifestations of cartilage and bone erosions, joint deformity,[1] stiffness, swelling, pain and joint function loss.[8,9] Natural TB was used to treat RA and osteoporosis in TCM.[16] However, TB substitute JTG has been approved only to cure osteoporosis for years. To explore other potential applications of TB substitute JTG, the present study investigated the therapeutic effects of JTG on RA in CIA animal model for the first time. Our results demonstrated that JTG possesses definite anti-arthritic properties (Figure 5A–C) and also mitigates deterioration of bone tissue in inflammatory joints (Figures 5F, 6F and 7), reverses the alteration of metabolic profiles (Table 2, Figure 10), especially the ammonia acid metabolism in CIA rats.

CIA rat is an established model for investigating the pathology and treatment of RA.[56] In the CIA model, arthritis is induced in rats by immunostimulating with heterologous CII in the adjuvant.[56] The primary pathological features of CIA are proliferative synovitis with infiltration of polymorphonuclear and mononuclear cells, pannus formation, cartilage degradation and erosion of bone.[57] Nevertheless, paw swelling and arthritis score, which are featured simple, sensitive and rapid, are commonly used to evaluate the severity of arthritis and the anti-arthritic activity of drugs.[42,58] In this study, CIA rats had been treated with JTG from day 28 to 69 after being injected with CII twice. It was found that both the diameter of paw joint and the arthritic score were reduced apparently in rats treated with JTG, as compared with CIA rats (Figure 5A–C). The remission effect of JTG on RA and associated bone deterioration was further confirmed by the results of histopathology observation and bone micro-architecture scanning, according to which it was indicated that JTG apparently reduced severity of synovial hyperplasia, cartilage and bone deterioration (Figures 5F, 6

**Table 2** Potential Biomarkers Identified in Rat Serum

| No. | Metabolite Identification | m/z | ESI | Normal vs CIA Model | | CIA Model vs JTG-360mg/kg | |
|---|---|---|---|---|---|---|---|
| | | | | FC | Trend | FC | Trend |
| 1 | 4,7,10,13,16,19-Docosahexaenoic acid | 327.2320 | [M-H]- | 0.69 | ↑* | 225.06 | ↓** |
| 2 | Gamma-L-Glutamyl-L-phenylalanine | 295.1334 | [M+H] + | 2.69 | ↓** | 0.37 | ↑* |
| 3 | L-Tyrosine | 182.0808 | [M+H] + | 1.81 | ↓** | 0.60 | ↑** |
| 4 | Lys-Thr | 230.1496 | [M+H] + | 1.77 | ↓** | 0.64 | ↑* |
| 5 | Arg-Met | 305.1452 | [M+H] + | 1.75 | ↓* | 0.60 | ↑** |
| 6 | Arg-Thr | 339.1767 | [M+H] + | 1.99 | ↓** | 0.47 | ↑** |
| 7 | Ile-Tyr | 294.1566 | [M+H] + | 1.93 | ↓** | 0.33 | ↑** |
| 8 | Leu-Thr | 296.1603 | [M+H] + | 2.07 | ↓** | 0.32 | ↑** |
| 9 | Val-Pro | 278.1500 | [M+H] + | 1.82 | ↓** | 0.35 | ↑** |
| 10 | N-Acetylaspartylglutamate | 305.1041 | [M+H] + | 2.10 | ↓** | 0.36 | ↑** |
| 11 | Glutaraldehyde | 123.0435 | [M+H] + | 1.41 | ↓* | 0.80 | ↑* |
| 12 | Dopamine | 136.0753 | [M+H] + | 1.44 | ↓* | 0.81 | ↑** |
| 13 | Cytidine | 244.0940 | [M-H]- | 0.72 | ↑** | 1.25 | ↓* |
| 14 | D-Ribose | 149.0446 | [M-H]- | 1.57 | ↓** | 35.52 | ↓** |
| 15 | 2-hydroxy-butanoic acid | 103.0394 | [M-H]- | 0.74 | ↑** | 0.01 | ↑** |
| 16 | L-Citrulline | 174.0915 | [M-H]- | 2.00 | ↓* | 0.16 | ↑** |
| 17 | L-Galactono-1,4-lactone | 237.1483 | [M-H]- | 0.73 | ↑* | 0.01 | ↑** |
| 18 | Dihydroxyacetone | 71.0136 | [M-H]- | 1.73 | ↓** | 1.95 | ↓** |
| 19 | D-Quinovose | 223.0815 | [M-H]- | 0.34 | ↑** | 6.09 | ↓** |
| 20 | 3-Methylhistidine | 170.0922 | [M+H] + | 0.62 | ↑** | 0.74 | ↑** |
| 21 | Val-Tyr | 280.1410 | [M+H] + | 1.63 | ↓** | 0.46 | ↑** |
| 22 | Phe-Tyr | 328.1397 | [M+H] + | 1.71 | ↓* | 0.36 | ↑** |
| 23 | 16-Hydroxypalmitic acid | 271.2266 | [M-H]- | 0.51 | ↑* | 0.14 | ↑** |
| 24 | Ribothymidine | 259.0931 | [M+H] + | 1.24 | ↓** | 0.72 | ↑** |
| 25 | N-Acetylglutamine | 233.0510 | [M+H] + | 1.36 | ↓** | 0.72 | ↑** |
| 26 | Taurine | 126.0223 | [M+H] + | 0.64 | ↑** | 1.71 | ↓** |
| 27 | Nicotinate | 124.0384 | [M+H] + | 2.65 | ↓* | 0.35 | ↑* |
| 28 | Acetylglycine | 118.0493 | [M+H] + | 1.39 | ↓** | 0.57 | ↑** |
| 29 | Alpha-Tocopherol | 430.3881 | [M+H] + | 0.53 | ↑* | 0.52 | ↑* |
| 30 | Dimethylglycine | 104.0704 | [M+H] + | 0.60 | ↑** | 1.40 | ↓* |
| 31 | sn-Glycerol 3-phosphoethanolamine | 214.0476 | [M-H]- | 0.61 | ↑* | 0.71 | ↑* |
| 32 | Stearoylcarnitine | 428.3663 | [M+H] + | 0.56 | ↑* | 0.54 | ↑* |
| 33 | Tyramine | 120.0813 | [M+H] + | 0.74 | ↑* | 1.12 | ↓ |
| 34 | Ile-Ala | 203.1389 | [M+H] + | 1.93 | ↓** | 0.85 | ↑ |
| 35 | L-Asparagine | 131.0455 | [M-H]- | 0.79 | ↑** | 0.93 | ↑ |
| 36 | Arachidonic Acid | 305.2435 | [M+H] + | 0.69 | ↑** | 1.12 | ↓ |
| 37 | N4-Acetylcytidine | 286.1036 | [M+H] + | 0.65 | ↑* | 1.04 | ↓ |
| 38 | Histamine | 112.0863 | [M+H] + | 0.52 | ↑* | 0.91 | ↑ |

**Notes:** FC was calculated based on mean ratios for Normal vs CIA model, or CIA model vs JTG-360mg/kg. The icons↑,↓ of trend represent up-regulation and down-regulation between the two groups; meanwhile * and ** represent change significance $P < 0.05$ and $P < 0.01$.

and 7), exhibiting that JTG significantly relieved the RA symptoms in CIA-induced arthritic rats.

Pro-inflammatory cytokines such as IL-6 and IL-1β are known to play primary roles in mediating the pathological processes of inflammation and tissue destruction in RA.[59] Too many pro-inflammatory cytokines aggravate the pain and deterioration of bone and cartilage.[60] In this study, serum IL-6 level (Figure 5D) has been decreased significantly ($P < 0.05$) in JTG treated CIA rats, whereas serum IL-1β level (Figure 5E) in those showed the go-down trend without significant differences, which might be due to the bigger SD. In other words, the tendency of alteration in serum levels of IL-6 and IL-1β also exhibited that JTG attenuated the symptom of RA by inhibiting the inflammatory cytokine level.

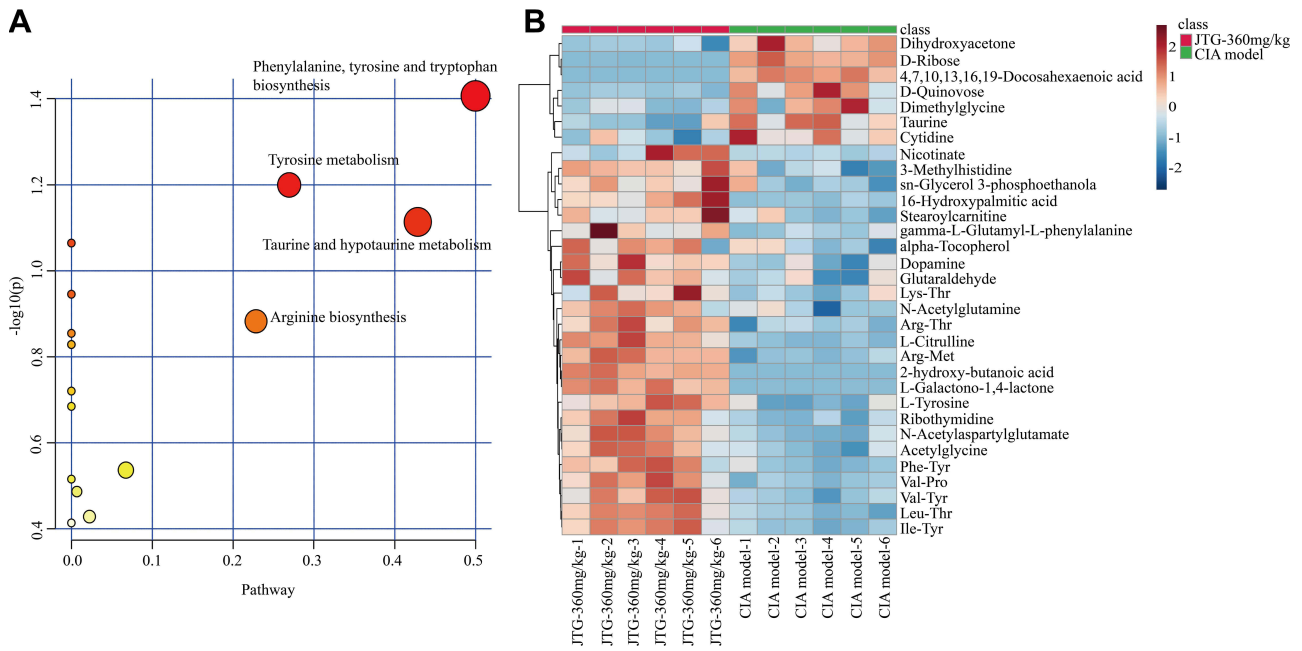


**Figure 10** The pathway impact prediction of MetaboAnalyst 5.0 online database between CIA model and JTG-360 mg/kg groups: (**A**) bubble diagram. Bubble color represents the *P*-value: deeper colors represent smaller *P* -values, indicating larger differences. The size of the bubble represents the impact of the pathway during topological analysis. Larger size represents a higher impact; (**B**) heat map of the differential metabolites in CIA model and JTG-360 mg/kg groups. Each cell in the heat map represents the fold change between the two groups: blue color represents the metabolite expression down-regulation, and red color represents the metabolite expression up-regulation.

Considering that thymus and spleen are two major organs of the body's immune system, their relative weights are commonly used as the preliminary indicators to evaluate the immune-regulatory activity of tested substrate.[61] This study presented that spleen index is slightly increased in CIA rats compared with those of normal rats (Figure 4B), but less changed in JTG treated rats. That may suggest that JTG do not produce immune-regulatory effects through spleen cells. Nevertheless, the thymus index was decreased ($P < 0.01$) in CIA rats compared with those of normal rats (Figure 4C), and JTG increased ($P < 0.05$) the thymus index in CIA rats. However, the reported results of the thymus index and the spleen index in CIA rats were not consistent in different literature.[11,62–65] So that it is worthy to further study on the effects of CII on thymus and spleen.

The inflammation reaction of RA often causes deterioration of bone microstructure in RA patients.[66] We specifically focused on the distal femur to assess the effects of synovial inflammation on the joint structure. At the end, we found that bone mineral density (Figure 7A) was decreased dramatically ($P < 0.01$), and microstructure was eroded in the bone tissue of inflammation joint of CIA rats. Consistent with the reduction of inflammation, BMD and other bone parameters (Figure 7) were significantly improved after JTG treatment. Furthermore, bone metabolism associated biomarkers are commonly used to assess the characteristics of bone-related disorders. CTX is the degradation products of bone collagen,[67] and the elevated levels of CTX-1 showed bone loss in CIA rats (Figure 6C). OCN is the biomarker of osteoblastic bone formation,[68] and TRAP, RANKL and OPG are indicators of osteoclastic bone resorption.[60] The alteration of TRAP in serum levels ($P < 0.01$) (Figure 6A) indicated that bone injury in CIA rats is predominantly caused by the increase in osteoclastic bone resorption, and JTG attenuated the deterioration of bone by inhibiting bone resorption. The bone deterioration occurs in the late stage of RA, and the duration of our experiment is 69 days, this may explain the results that serum levels of RANKL (Figure 6B) and OPG (Figure 6E) were not significantly altered in CIA rats. In brief, the results of bone parameters combined with serum biomarker demonstrated that JTG mitigated the bone deterioration by inhibiting osteoclastic bone resorption in CIA rats.

Serum metabolites can reflect changes in the endogenous metabolite-associated metabolic pathways of the system, organ or the whole organism. Herein, we used UPLC-Q-TOF-MS to conduct a serum metabolomic study to assess the efficacy and the underlying mechanism of JTG

for treating rheumatoid arthritis in CIA rats, and identified 38 differentially expressed metabolites between the normal and model groups (Table 2). These differential metabolites were mainly related to phenylalanine, tyrosine and tryptophan biosynthesis. The levels of some amino acids including Lys-Thr, Arg-Met, Arg-Thr, Ile-Tyr, Leu-Thr, Val-Pro, L-Citrulline, 3-Methylhistidine, Val-Tyr, Phe-Tyr, Dimethylglycine, L-Asparagine and Ile-Ala were decreased in CIA rats, which is consistent with previous report in the literature.[69] JTG reversed the alteration of the above amino acids, suggesting that JTG might be involved in the amino acid metabolism. Metabolomics analysis of the CIA rat serum demonstrated that several distinct metabolic pathways were involved in the progress of RA (Figure S3). The results showed that JTG treatment in three doses were all mainly associated with the involvement of phenylalanine, tyrosine, and tryptophan biosynthesis pathway (180 mg/kg JTG in Figure S4D, 360 mg/kg JTG in Figure 10A, and 720 mg/kg JTG in FigureS5D). Some differential metabolites were closely associated with inflammation in different metabolite pathways. The increased level of phenylalanine was correlated with higher pro-inflammatory, innate, and adaptive T lymphocyte immune cytokines such as IL-8 and IL-10.[70] And the conversion of phenylalanine to tyrosine is also affected by inflammation and immune activation.[71] It was reported that phenylalanine, tyrosine, and tryptophan biosynthesis pathway may be implicated in the neurotransmitter release and pain conductivity in complete Freund's adjuvant-induced chronic inflammation pain mice.[72] Guo et al[73] used metabolomics technique to analyze the acupuncture-induced improvement of symptoms of RA patients, and the result showed that acupuncture can relieve symptoms of RA patients, which may involve phenylalanine, tyrosine, and tryptophan biosynthesis pathway. Furthermore, phenylalanine, tyrosine, and tryptophan biosynthesis pathway were correlated with dermatomyositis,[74] chronic low-grade inflammation[75] and neurological inflammatory disease.[76] On the other hand, Refaey et al[77] reported that aromatic amino acid (phenylalanine, tyrosine, and tryptophan) supplementation prevented bone loss in an aging C57BL/6 mouse model. The pathway may also be related to glucocorticoid-induced osteoporosis and ovarian osteoporosis.[78,79] Another study[80] reported that the serum profile of amino acids was associated with BMD decline and fracture risk, and the serum level of phenylalanine and tyrosine was decreased in osteoporotic men and women. It was found in ours study that the level of phenylalanine and tyrosine was reduced in CIA rats, and JTG could regulate the serum level of the two amino acids in CIA rats, suggesting that the effect of JTG in alleviating inflammation and bone deterioration in CIA rats may be related to phenylalanine, tyrosine, and tryptophan biosynthesis. Otherwise, other metabolic pathways were not significant, but it also might affect the inflammation or bone metabolism. Taurine is a semi-essential sulfur-containing β-amino acid existing at high concentrations in most cells of all animal species.[81] Human taurine is formed from methionine and cysteine metabolism via hypotaurine in hepatocytes.[82] Metabolomics studies have demonstrated that taurine is increased in osteoarthritis versus control serum.[83] Taurine is involved in the pathogenesis of subchondral bone sclerosis, a feature of osteoarthritis.[84,85] It is possible that the increased level of taurine identified in this study may be a consequence of increased subchondral bone sclerosis in RA samples.[86] Arachidonic acid, a component that is released from cellular membrane would be metabolized as a variety of metabolites.[87] It was reported that reprogramming cyclooxygenase-2, 5-lipoxygenase, and cytochrome P450 4A-mediated arachidonic acid metabolism in macrophages by salidroside ameliorates monosodium urate crystal-induced inflammation.[88,89] Furthermore, arachidonic acid metabolism involve in the localization of critical enzymes during the initial and regenerative phases of mouse femur fracture healing.[90] In addition to amino acid metabolism, some metabolites related to inflammation, such as L-citrulline, cytidine, N4-acetylcytidine and stearoylcarnitine,[91,92] underwent changes in CIA rats. Some metabolites associated with relieving pain such as N-Acetylaspartylglutamate and N-Acetylglutamine also underwent change in CIA rats. In short, the results showed that the levels of serum biomarkers in rats administrated with JTG have remarkable reversed compared with those in CIA model rats.

As we mentioned, JTG is prepared from animals bone extract.[19] Another similar product is Sailonggu (SLG), which is an extract prepared from the whole skeleton of the zokor, a Tibetan plateau Rodentia animal named Myospalax baileyi Thomas.[93] Both JTG and SLG have the effects of anti-rheumatoid arthritis, anti-osteoporosis, analgesics and anti-inflammation.[19,93–96] SLG has been reported to significantly attenuate symposium of arthritis in CIA mice and CFA-induced arthritis model mice, and also significantly inhibit the proliferation of spleen cells and the production of IL-2, IFN-γ, L-12p40, IL-1, IL-6 and TNF-α cytokines in arthritic mice at dose of 180 and

360 mg/kg.[96] JTG could also decrease the paw swelling and arthritic score in CIA model rats at doses of 180, 360 and 720 mg/kg as found in this study, but had no effects on the production of IL-1β. SLG has been shown to attenuate osteoclast differentiation through RANKL-induced NFAT pathways.[93] JTG can inhibit the bone loss in CIA rats as reported in this study, and also prevent bone loss in ovariectomized rats. Therefore, JTG and SLG have definitely anti-arthritic and anti-osteoporotic activities, their differences in characteristics and mechanisms are not clear, and need further investigated.

There are still some limitations of this study need to be further explored. First, JTG often causes thirst and dryness in osteoporotic patients,[97] which might reflect some side effects of JTG in patients. But in this study, we did not observe the water intake of rats. Secondly, we analyzed the serum metabolic profile changes in CIA rats at the end point, but our results lack the observation of dynamic changes in metabolic profile at different times. Thirdly, we found some metabolites are altered in CIA rats and the reversal effects of JTG, and further prospective study could be deeper in clarifying the association of these metabolites with the intervention mechanism of JTG on RA. Finally, we revealed the peptides and protein profiles and their biological functions, but the questions of which peptides and proteins may play critical roles in the treatment of RA are still not clarified.

## Conclusions

In the present study, we used pharmacological experiments and UPLC-Q/TOF-MS-based metabolomics analysis to evaluate the effect and underlying mechanism of JTG on RA and its associated bone deterioration in CIA rats, and found that JTG was able to attenuate the paw swelling and improve the cancellous bone structure, enhance BMD, and restore bone metabolism homeostasis. Metabolomics profiling suggested that the effect of JTG in alleviating RA and associated bone deterioration may involve in the biosynthesis of phenylalanine, tyrosine and tryptophan. The above findings demonstrated that approved drug JTG, a TB substitute, was proved to be a potential candidate for RA therapy.

## Abbreviations

ACN, acetonitrile; AGC, automatic gain control; ANOVA, one- or two-way analysis of variance; BMD, bone mineral density; BS/BV, bone surface to bone volume; BVF, bone volume fraction; CIA, collagen-induced arthritis; CII, type II collagen; CITES, Convention on International Trade in Endangered Species of Wild Fauna and Flora; CMC-Na, carboxymethylcellulose sodium; CTX-I, C-Telopeptide of type I collagen; EDTA, ethylene diamine tetra acetic acid; ELISA, enzyme-linked immunosorbent assay; HMDB, Human Metabolome Database; IFA, Freund's adjuvant incomplete; IL-1β, interleukin 1 beta; IL-6, interleukin-6; JTG, Jin-Tian-Ge; LSD, least significance differences; MS, mass Spectrometry; MTX, methotrexate; NIH, National Institute of Health; OCN, osteocalcin; OPG, osteoprotegerin; OPLS-DA, orthogonal projections to latent structures discriminant analysis; PCA, principal components analysis; PC1, principal components 1; PC2, principal components 2; QC, quality control; RA, rheumatoid arthritis; RANKL, receptor activator of nuclear factor kappa B ligand; SPSS, statistical product and service solutions; TB, tiger bone; Tb.N, trabecular number; Tb.Sp, trabecular separation; Tb.Th, trabecular thickness; TCM, traditional Chinese medicine; TIC, total ions chromatographies; TRAP, tartrate resistant acid phosphatase; TV, total volume of interest; UPLC-MS, ultra-high liquid chromatography-quadrupole-time of flight-mass spectrometry; VIP, variable importance in projection.

## Institutional Review Board Statement

The study was conducted according to the guidelines of the National Institute of Health (NIH), and all experimental protocols associated with this study were approved by the Bioethics Committee of Zhejiang Chinese Medical University (Approval No. IACUC-20200420-04).

## Acknowledgments

We appreciate the support from the Public Research Platform of the Academy of Chinese Medical Sciences, Zhejiang Chinese Medical University and the BIOTREE company (Shanghai, China).

## Funding

This work was supported by the National Natural Science Foundation of China (Grant No. 81973571) and YUANZHI Outstanding Youth Research Foundation of Zhejiang Chinese Medical University (2019).

## Disclosure

Na Wang is an employee of Ginwa Enterprise (Group) INC. The authors report no other potential conflicts of interest in this work.

## References


1. Firestein GS. Evolving concepts of rheumatoid arthritis. *Nature*. 2003;423(6937):356–361. doi:10.1038/nature01661
2. Deane KD, Demoruelle MK, Kelmenson LB, Kuhn KA, Norris JM, Holers VM. Genetic and environmental risk factors for rheumatoid arthritis. *Best Pract Res Clin Rheumatol*. 2017;31(1):3–18. doi:10.1016/j.berh.2017.08.003
3. Liu Y, Aryee MJ, Padyukov L, et al. Epigenome-wide association data implicate DNA methylation as an intermediary of genetic risk in rheumatoid arthritis. *Nat Biotechnol*. 2013;31(2):142–147. doi:10.1038/nbt.2487
4. Viatte S, Massey J, Bowes J, et al. Replication of associations of genetic loci outside the HLA region with susceptibility to anti-cyclic citrullinated peptide-negative rheumatoid arthritis. *Arthritis Rheumatol*. 2016;68(7):1603–1613. doi:10.1002/art.39619
5. Okada Y, Wu D, Trynka G, et al. Genetics of rheumatoid arthritis contributes to biology and drug discovery. *Nature*. 2014;506(7488):376–381. doi:10.1038/nature12873
6. Stahl EA, Raychaudhuri S, Remmers EF, et al. Genome-wide association study meta-analysis identifies seven new rheumatoid arthritis risk loci. *Nat Genet*. 2010;42(6):508–514. doi:10.1038/ng.582
7. Smolen JS, Aletaha D, McInnes IB. Rheumatoid arthritis. *Lancet*. 2016;388(10055):2023–2038. doi:10.1016/S0140-6736(16)30173-8
8. Di Paola R, Cuzzocrea S. Predictivity and sensitivity of animal models of arthritis. *Autoimmun Rev*. 2008;8(1):73–75. doi:10.1016/j.autrev.2008.07.029
9. Dinser R. Animal models for arthritis. *Best Pract Res Clin Rheumatol*. 2008;22(2):253–267. doi:10.1016/j.berh.2008.01.007
10. Chen L, Li J, Ke X, et al. The therapeutic effects of Periploca forrestii Schltr. Stem extracts on collagen-induced arthritis by inhibiting the activation of Src/NF-kappaB signaling pathway in rats. *J Ethnopharmacol*. 2017;202:12–19. doi:10.1016/j.jep.2017.03.005
11. Jing R, Ban Y, Xu W, et al. Therapeutic effects of the total lignans from Vitex negundo seeds on collagen-induced arthritis in rats. *Phytomedicine*. 2019;58:152825. doi:10.1016/j.phymed.2019.152825
12. Smolen JS, Landewe R, Breedveld FC, et al. EULAR recommendations for the management of rheumatoid arthritis with synthetic and biological disease-modifying antirheumatic drugs: 2013 update. *Ann Rheum Dis*. 2014;73(3):492–509. doi:10.1136/annrheumdis-2013-204573
13. Singh JA, Saag KG, Bridges SL Jr, et al. 2015 American college of rheumatology guideline for the treatment of rheumatoid arthritis. *Arthritis Rheumatol*. 2016;68(1):1–26. doi:10.1002/art.39480
14. Silvagni E, Giollo A, Sakellariou G, et al. One year in review 2020: novelties in the treatment of rheumatoid arthritis. *Clin Exp Rheumatol*. 2020;38(2):181–194.
15. Pimanov SI, Makarenko EV, Dikareva EA. [Adherence with proton pump inhibitor therapy, by continuously taking nonsteroidal anti-inflammatory drugs]. *Ter Arkh*. 2015;87(4):58–61. Russian. doi:10.17116/terarkh201587458-61
16. Si SZ, Luo X. *Compendium of Materia Medica Bencao Gangmu Book*. Foreign Languages Press; 2003.
17. Gratwicke B, Mills J, Dutton A, et al. Attitudes toward consumption and conservation of tigers in China. *PLoS One*. 2008;3(7):e2544. doi:10.1371/journal.pone.0002544
18. Guo XQ, Ye J, Li JG. [Research progress on the skeleton of tiger and its substitute]. *J Shaanxi Norm Univ Nat Sci Ed*. 2006;S1:218–221. Chinese. doi:10.15983/j.cnki.jsnu.2006.s1.055
19. Sun J, Yang XG, Hu YC. Efficacy of jintiange capsules in the treatment of osteoporosis: a network meta-analysis. *Orthop Surg*. 2019;11(2):176–186. doi:10.1111/os.12439
20. Fan YM, Li RF. [Effect of artificial tiger bone powder on retinoic acid-induced osteoporosis in rat]. *Pharmacol Clin Chin Mater Med*. 2001;17:13–14. Chinese.
21. Wu LS, Sun SC, Shi GT, Wang HM, Shen L, Tao YL. [Clinical study on effect of JINTIANGE capsules for treatment of primary osteoporosis]. *Chin J Osteoporos*. 2005;4:82–87. Chinese.
22. Zhao Y, Li AQ, Ni LG, Wang W. [The research progress of tiger bone and artificial tiger bone for the treatment of osteoporosis]. *Chin J Osteoporos*. 2012;18:95–98. Chinese.
23. Zhao J, Zeng L, Wu M, et al. Efficacy of Chinese patent medicine for primary osteoporosis: a network meta-analysis. *Complement Ther Clin Pract*. 2021;44:101419. doi:10.1016/j.ctcp.2021.101419
24. Ren S, Jiao G, Zhang L, You Y, Chen Y. Bionic tiger-bone powder improves bone microstructure and bone biomechanical strength of ovariectomized rats. *Orthop Surg*. 2021;13(3):1111–1118. doi:10.1111/os.12954
25. Li Y, Zhang Z, Cui F, et al. Traditional Chinese medicine bionic tiger bone powder for the treatment of AI-associated musculoskeletal symptoms. *Evid Based Complement Alternat Med*. 2017;2017:2478565. doi:10.1155/2017/2478565
26. Xie TG. [Jintiange capsules combined with Zoledronic acid injection treating postmenopausal diabetic osteoporosis in terms of bone mineral density and laboratory indexes]. *J Chin Prescription Drug*. 2018;16(3):60–61. Chinese.
27. Zhang J, Wu LS, Sun SC, et al. [Clinical study on effect of JINTIANGE capsules for treatment of primary osteoporosis. *Chin J Osteoporosis*. 2005;11(4):490–495]. Chinese.
28. [Guideline of diagnosis and treatment of primary osteoporosis (2017)]. *Chin J Osteoporos Bone Mineral Res*. 2017;10:413–444. Chinese.
29. Takahashi S, Saegusa J, Onishi A, Morinobu A. Biomarkers identified by serum metabolomic analysis to predict biologic treatment response in rheumatoid arthritis patients. *Rheumatology*. 2019;58(12):2153–2161. doi:10.1093/rheumatology/kez199
30. Wang Z, Chen Z, Yang S, et al. (1)H NMR-based metabolomic analysis for identifying serum biomarkers to evaluate methotrexate treatment in patients with early rheumatoid arthritis. *Exp Ther Med*. 2012;4(1):165–171. doi:10.3892/etm.2012.567
31. Li J, Che N, Xu L, et al. LC-MS-based serum metabolomics reveals a distinctive signature in patients with rheumatoid arthritis. *Clin Rheumatol*. 2018;37(6):1493–1502. doi:10.1007/s10067-018-4021-6
32. Zabek A, Swierkot J, Malak A, et al. Application of (1)H NMR-based serum metabolomic studies for monitoring female patients with rheumatoid arthritis. *J Pharm Biomed Anal*. 2016;117:544–550. doi:10.1016/j.jpba.2015.10.007
33. Xia T, Dong X, Jiang Y, et al. Metabolomics profiling reveals rehmanniae radix preparata extract protects against glucocorticoid-induced osteoporosis mainly via intervening steroid hormone biosynthesis. *Molecules*. 2019;24(2):253. doi:10.3390/molecules24020253
34. Ye M, Zhang C, Jia W, et al. Metabolomics strategy reveals the osteogenic mechanism of yak (Bos grunniens) bone collagen peptides on ovariectomy-induced osteoporosis in rats. *Food Funct*. 2020;11(2):1498–1512. doi:10.1039/c9fo01944h
35. Shi H, Zhao T, Li Y, et al. Velvet antler ameliorates cardiac function by restoring sarcoplasmic reticulum Ca(2+)-ATPase activity in rats with heart failure after myocardial infarction. *Front Pharmacol*. 2021;12:621194. doi:10.3389/fphar.2021.621194
36. Xiao X, Xu S, Li L, et al. The effect of velvet antler proteins on cardiac microvascular endothelial Cells challenged with ischemia-hypoxia. *Front Pharmacol*. 2017;8:601. doi:10.3389/fphar.2017.00601
37. Dai Q, Zhou D, Xu L, Song X. Curcumin alleviates rheumatoid arthritis-induced inflammation and synovial hyperplasia by targeting mTOR pathway in rats. *Drug Des Devel Ther*. 2018;12:4095–4105. doi:10.2147/DDDT.S175763
38. Gao Q, Qin H, Zhu L, Li D, Hao X. Celastrol attenuates collagen-induced arthritis via inhibiting oxidative stress in rats. *Int Immunopharmacol*. 2020;84:106527. doi:10.1016/j.intimp.2020.106527

39. Xia ZB, Yuan YJ, Zhang QH, Li H, Dai JL, Min JK. Salvianolic acid B suppresses inflammatory mediator levels by downregulating NF-kappaB in a rat model of rheumatoid arthritis. *Med Sci Monit*. 2018;24:2524–2532. doi:10.12659/msm.907084
40. Pei B, Chen K, Zhou S, Min D, Xiao W. IL-38 restrains inflammatory response of collagen-induced arthritis in rats via SIRT1/HIF-1alpha signaling pathway. *Biosci Rep*. 2020;40(5). doi:10.1042/BSR20182431
41. Zhang LL, Wei W, Yan SX, Hu XY, Sun WY. [Therapeutic effects of glucosides of Chaenomeles speciosa on collagen-induced arthritis in mice]. *Acta Pharmacol Sin*. 2004;25(11):1495–1501. Chinese.
42. Wang Q, Ye C, Sun S, et al. Curcumin attenuates collagen-induced rat arthritis via anti-inflammatory and apoptotic effects. *Int Immunopharmacol*. 2019;72:292–300. doi:10.1016/j.intimp.2019.04.027
43. Liu L, Tian YG, Su XH, et al. [Comparative study on dose-toxicity-effect of Tripterygium Glycosides tablets and Tripterygium wilfordii tablets on CIA model rats]. *Zhongguo Zhong Yao Za Zhi*. 2019;44(16):3502–3511. Chinese. doi:10.19540/j.cnki.cjcmm.20190703.401
44. Engelke K, Libanati C, Fuerst T, Zysset P, Genant HK. Advanced CT based in vivo methods for the assessment of bone density, structure, and strength. *Curr Osteoporos Rep*. 2013;11(3):246–255. doi:10.1007/s11914-013-0147-2
45. Parfitt AM, Mathews CH, Villanueva AR, Kleerekoper M, Frame B, Rao DS. Relationships between surface, volume, and thickness of iliac trabecular bone in aging and in osteoporosis. Implications for the microanatomic and cellular mechanisms of bone loss. *J Clin Invest*. 1983;72(4):1396–1409. doi:10.1172/JCI111096
46. Muller R, Ruegsegger P. Three-dimensional finite element modelling of non-invasively assessed trabecular bone structures. *Med Eng Phys*. 1995;17(2):126–133. doi:10.1016/1350-4533(95)91884-j
47. Lorensen WE, Cline HE. Marching cubes: a high resolution 3D surface construction algorithm. *Comput Graph (ACM)*. 1987;21(4):163–169. doi:10.1145/37402.37422
48. Pritchard JM. A new method for the model-independent assessment of thickness in three-dimensional images (vol 185, pg 67, 1997). *Arthrit Care Res*. 2012;64(6):944. doi:10.1002/acr.21718
49. Danielson PE. Euclidean distance mapping. *Comp Vision Graph Image Process*. 1980;14(3):227–248. doi:10.1016/0146-664X(80)90054-4
50. Zeng C, Lin H, Liu Z, Liu Z. Analysis of young shoots of 'Anji Baicha' (Camellia sinensis) at three developmental stages using non-targeted LC-MS-based metabolomics. *J Food Sci*. 2019;84(7):1746–1757. doi:10.1111/1750-3841.14657
51. Silalahi DD, Midi H, Arasan J, Mustafa MS, Caliman JP. Robust wavelength selection using filter-wrapper method and input scaling on near infrared spectral data. *Sensors*. 2020;20(17):5001. doi:10.3390/s20175001
52. Bouxsein ML, Boyd SK, Christiansen BA, Guldberg RE, Jepsen KJ, Muller R. Guidelines for assessment of bone microstructure in rodents using micro-computed tomography. *J Bone Miner Res*. 2010;25(7):1468–1486. doi:10.1002/jbmr.141
53. Bocca C, Le Paih V, Chao de la Barca JM, et al.A plasma metabolomic signature of Leber hereditary optic neuropathy showing taurine and nicotinamide deficiencies. *Hum Mol Genet*. 2021;30(1):21–29. doi:10.1093/hmg/ddab013
54. Gou XJ, Gao S, Chen L, Feng Q, Hu YY. A metabolomic study on the intervention of traditional Chinese medicine Qushi Huayu Decoction on rat model of fatty liver induced by high-fat diet. *Biomed Res Int*. 2019;2019:5920485. doi:10.1155/2019/5920485
55. Zhu Y, Guo Z, Zhang L, et al. System-wide assembly of pathways and modules hierarchically reveal metabolic mechanism of cerebral ischemia. *Sci Rep*. 2015;5(1):17068. doi:10.1038/srep17068
56. Liu H, Zhao J, Su M, Tian X, Lai LL. Recombinant CD300c-Ig fusion protein attenuates collagen-induced arthritis in mice. *Rheumatology*. 2021. doi:10.1093/rheumatology/keab450
57. Gravallese EM. Bone destruction in arthritis. *Ann Rheum Dis*. 2002;61(Suppl 2):ii, 84–86. doi:10.1136/ard.61.suppl_2.ii84
58. Petchi RR, Vijaya C. Anti-diabetic and anti-arthritic potential of Glycosmis pentaphylla stem bark in FCA induced arthritis and streptozotocin induced diabetic rats. *Pharmacol Int J Pharma Biol Sci*. 2012;3:328–336.
59. McInnes IB, Schett G. Cytokines in the pathogenesis of rheumatoid arthritis. *Nat Rev Immunol*. 2007;7(6):429–442. doi:10.1038/nri2094
60. Hemshekhar M, Thushara RM, Kumar SKN, et al. Bone degeneration, inflammation and secondary complications of arthritis: potential targets and their Natural inhibitors. *Mini Rev Med Chem*. 2018;18(3):244–275. doi:10.2174/1389557517666170315144233
61. Jiang CP, He X, Yang XL, et al. Anti-rheumatoid arthritic activity of flavonoids from Daphne genkwa. *Phytomedicine*. 2014;21(6):830–837. doi:10.1016/j.phymed.2014.01.009
62. Jia N, Chu W, Li Y, et al. Iridoid glycosides from the flowers of Gentiana macrophylla Pall. ameliorate collagen-induced arthritis in rats. *J Ethnopharmacol*. 2016;189(1):1–9. doi:10.1016/j.jep.2016.05.027
63. Li X, Jiang C, Zhu W. Crocin reduces the inflammation response in rheumatoid arthritis. *Biosci Biotechnol Biochem*. 2017;81(5):891–898. doi:10.1080/09168451.2016.1263145
64. Wu L. [The gas-gai coupling switch of β2 adrenergic receptor promotes the activation of rheumatic synoviocytes and the regulatory effect of CP-25]. Anhui Medical University; 2015. Chinese.
65. Hu SS. [IL-6 promotes Th17 differentiation via inhibiting adenosine A3 receptor signaling in rats with collagen-induced arthritis]. Anhui Medical University; 2019. Chinese.
66. Finzel S, Ohrndorf S, Englbrecht M, et al. A detailed comparative study of high-resolution ultrasound and micro-computed tomography for detection of arthritic bone erosions. *Arthritis Rheum*. 2011;63(5):1231–1236. doi:10.1002/art.30285
67. Vasikaran S, Eastell R, Bruyere O, et al. Markers of bone turnover for the prediction of fracture risk and monitoring of osteoporosis treatment: a need for international reference standards. *Osteoporos Int*. 2011;22(2):391–420. doi:10.1007/s00198-010-1501-1
68. Komori T. Functions of osteocalcin in bone, pancreas, testis, and muscle. *Int J Mol Sci*. 2020;21(20):7513. doi:10.3390/ijms21207513
69. He M, Harms AC, van Wijk E, et al. Role of amino acids in rheumatoid arthritis studied by metabolomics. *Int J Rheum Dis*. 2019;22(1):38–46. doi:10.1111/1756-185X.13062
70. Chen WS, Wang CH, Cheng CW, et al. Elevated plasma phenylalanine predicts mortality in critical patients with heart failure. *ESC Heart Fail*. 2020;7(5):2884–2893. doi:10.1002/ehf2.12896
71. Murr C, Grammer TB, Meinitzer A, Kleber ME, Marz W, Fuchs D. Immune activation and inflammation in patients with cardiovascular disease are associated with higher phenylalanine to tyrosine ratios: the Ludwigshafen risk and cardiovascular health study. *J Amino Acids*. 2014;2014:783730. doi:10.1155/2014/783730
72. Zhang W, Lyu J, Xu J, et al. The related mechanism of complete Freund's adjuvant-induced chronic inflammation pain based on metabolomics analysis. *Biomed Chromatogr*. 2021;35(4):e5020. doi:10.1002/bmc.5020
73. Guo YG, Sun GW, Yang L, Li C, Yang J. [Differential metabolites and metabolic pathways involving acupuncture-induced improvement of rheumatoid arthritis patients based on gas chromatography-mass spectrometry]. *Cupunct Res*. 2021;46(2):145–151. Chinese.
74. Zhang T, Xu J, Liu Y, Liu J. Metabolomic profiling for identification of potential biomarkers in patients with dermatomyositis. *Metabolomics*. 2019;15(5):77. doi:10.1007/s11306-019-1539-9
75. Capuron L, Schroecksnadel S, Feart C, et al. Chronic low-grade inflammation in elderly persons is associated with altered tryptophan and tyrosine metabolism: role in neuropsychiatric symptoms. *Biol Psychiatry*. 2011;70(2):175–182. doi:10.1016/j.biopsych.2010.12.006
76. Strasser B, Sperner-Unterweger B, Fuchs D, Gostner JM. Mechanisms of inflammation-associated depression: immune influences on tryptophan and phenylalanine metabolisms. *Curr Top Behav Neurosci*. 2017;31:95–115. doi:10.1007/7854_2016_23

77. Refaey ME, Zhong Q, Ding KH, et al. Impact of dietary aromatic amino acids on osteoclastic activity. *Calcif Tissue Int*. 2014;95(2):174–182. doi:10.1007/s00223-014-9878-z
78. Xu Y, Chen S, Yu T, Qiao J, Sun G. High-throughput metabolomics investigates anti-osteoporosis activity of oleanolic acid via regulating metabolic networks using ultra-performance liquid chromatography coupled with mass spectrometry. *Phytomedicine*. 2018;51:68–76. doi:10.1016/j.phymed.2018.09.235
79. Tao Y, Chen X, Li W, et al. Global and untargeted metabolomics evidence of the protective effect of different extracts of Dipsacus asper Wall. ex C.B. Clarke on estrogen deficiency after ovariectomia in rats. *J Ethnopharmacol*. 2017;199:20–29. doi:10.1016/j.jep.2017.01.050
80. Su Y, Elshorbagy A, Turner C, Refsum H, Chan R, Kwok T. Circulating amino acids are associated with bone mineral density decline and ten-year major osteoporotic fracture risk in older community-dwelling adults. *Bone*. 2019;129:115082. doi:10.1016/j.bone.2019.115082
81. Sturman JA. Taurine in development. *Physiol Rev*. 1993;73(1):119–147. doi:10.1152/physrev.1993.73.1.119
82. Bouckenooghe T, Remacle C, Reusens B. Is taurine a functional nutrient? *Curr Opin Clin Nutr Metab Care*. 2006;9(6):728–733. doi:10.1097/01.mco.0000247469.26414.55
83. Kang KY, Lee SH, Jung SM, Park SH, Jung BH, Ju JH. Downregulation of tryptophan-related metabolomic profile in rheumatoid arthritis synovial fluid. *J Rheumatol*. 2015;42(11):2003–2011. doi:10.3899/jrheum.141505
84. Li G, Ma Y, Cheng TS, et al. Identical subchondral bone microarchitecture pattern with increased bone resorption in rheumatoid arthritis as compared to osteoarthritis. *Osteoarthritis Cartilage*. 2014;22(12):2083–2092. doi:10.1016/j.joca.2014.08.015
85. Yang G, Zhang H, Chen T, et al. Metabolic analysis of osteoarthritis subchondral bone based on UPLC/Q-TOF-MS. *Anal Bioanal Chem*. 2016;408(16):4275–4286. doi:10.1007/s00216-016-9524-x
86. Anderson JR, Chokesuwattanaskul S, Phelan MM, et al. (1)H NMR metabolomics identifies underlying inflammatory pathology in osteoarthritis and rheumatoid arthritis synovial joints. *J Proteome Res*. 2018;17(11):3780–3790. doi:10.1021/acs.jproteome.8b00455
87. Kim Y, Gromovsky AD, Brown JM, Chung S. Gamma-tocotrienol attenuates the aberrant lipid mediator production in NLRP3 inflammasome-stimulated macrophages. *J Nutr Biochem*. 2018;58:169–177. doi:10.1016/j.jnutbio.2018.05.007
88. Yarla NS, Bishayee A, Sethi G, et al. Targeting arachidonic acid pathway by natural products for cancer prevention and therapy. *Semin Cancer Biol*. 2016;40–41:48–81. doi:10.1016/j.semcancer.2016.02.001
89. Liu Y, Tang H, Liu X, et al. Frontline science: reprogramming COX-2, 5-LOX, and CYP4A-mediated arachidonic acid metabolism in macrophages by salidroside alleviates gouty arthritis. *J Leukoc Biol*. 2019;105(1):11–24. doi:10.1002/JLB.3HI0518-193R
90. Lin HN, O'Connor JP. Immunohistochemical localization of key arachidonic acid metabolism enzymes during fracture healing in mice. *PLoS One*. 2014;9(2):e88423. doi:10.1371/journal.pone.0088423
91. Ham DJ, Gleeson BG, Chee A, et al. L-citrulline protects skeletal muscle cells from Cachectic stimuli through an iNOS-dependent mechanism. *PLoS One*. 2015;10(10):e0141572. doi:10.1371/journal.pone.0141572
92. Hoxha M. A systematic review on the role of eicosanoid pathways in rheumatoid arthritis. *Adv Med Sci*. 2018;63(1):22–29. doi:10.1016/j.advms.2017.06.004
93. Cui Y, Zhao X, Mei L, et al. [Osteon Myospalacem Baileyi attenuates osteoclast differentiation through RANKL induced NFAT pathways]. *J Ethnopharmacol*. 2018;213:65–71. doi:10.1016/j.jep.2017.10.007
94. Zhao XH, Jiang FQ, Yue HL, Shao Y, Tao YZ. [Study on pharmacodynamics of Myospalax fontaneieri extract on experimental rheumatoid arthritis]. *Chin Tradit Patent Med*. 2007;29(8):1221–1223. Chinese.
95. Zhao XH, Yue HL, Mei LJ, Shao Y, Tao YZ. [Therapeutic effects and mechanism of Myospalax fontaneieri extract on bovine type II collagen-induced mouse arthritis]. *Chin Pharm Bullet*. 2008;24(3):395–399. Chinese.
96. Zhao XH, Yue HL, Mei LJ, Shao Y, Tao YZ. [Effect of Myospalax fontaneieri bone extract on the function of CFA induced mice]. *Chin Tradit Patent Med*. 2008;30(3):330–332. Chinese.
97. Huang GP, Chen M, Liu XQ, Li J, Li TH. [Clinical observation of Jintiange capsules for postmenopausal osteoporosis]. *J Chin Med Mater*. 2017;40(4):970–972. Chinese.